

# DOPPLER: Dual-Policy Learning for Device Assignment in Asynchronous Dataflow Graphs

Xinyu Yao<sup>1</sup> Daniel Bourgeois<sup>1</sup> Abhinav Jain<sup>1</sup> Yuxin Tang<sup>1</sup> Jiawen Yao<sup>1</sup>  
 Zhimin Ding<sup>1</sup> Arlei Silva<sup>1</sup> Chris Jermaine<sup>1</sup>

<sup>1</sup>Rice University

{xy38, dcb10, aj70, yt33, jy75, zd21, arlei, cmj4}@rice.edu

## Abstract

We study the problem of assigning operations in a dataflow graph to devices to minimize execution time in a work-conserving system, with emphasis on complex machine learning workloads. Prior learning-based methods often struggle due to three key limitations: (1) reliance on bulk-synchronous systems like TensorFlow, which under-utilize devices due to barrier synchronization; (2) lack of awareness of the scheduling mechanism of underlying systems when designing learning-based methods; and (3) exclusive dependence on reinforcement learning, ignoring the structure of effective heuristics designed by experts. In this paper, we propose DOPPLER, a three-stage framework for training dual-policy networks consisting of 1) a SEL policy for selecting operations and 2) a PLC policy for placing chosen operations on devices. Our experiments show that DOPPLER outperforms all baseline methods across tasks by reducing system execution time and additionally demonstrates sampling efficiency by reducing per-episode training time.

## 1 Introduction

Existing systems for multi-GPU computing such as PyTorch [39], TensorFlow [1], and the JAX-based Google stack [17] proceed through a computation in lock-step, level-wise fashion. Consider the simple multi-layer perceptron  $f(f(X \times W_1) \times W_2)$  where  $X$  is a feature matrix,  $W_1$  and  $W_2$  are weight matrices, and  $f$  is a nonlinear function (e.g., ReLU). When a system such as JAX is used to implement this computation on a multi-GPU server, it will first compute  $X \times W_1$  using a set of pairwise matrix multiplies distributed over the server’s GPUs, followed by a bulk synchronous operation such as an all-reduce. After applying  $f$  to the result, there is another synchronous step where the result is multiplied by  $W_2$  via another set of pairwise multiplies, followed by another synchronous all-reduce. Finally,  $f$  is computed on the result.

The synchronous nature of the computation can result in idle computing resources and lost opportunities to speed up the computation. Neither all-reduce can begin until all of the pairwise matrix multiplications are complete. One slow multiplication will force the all-reduce to be delayed. Further, the all-reduce step is dominated by communication, during which time the GPUs are all underutilized.

It would be preferable to overlap the reduce operation with the matrix multiplications to the greatest extent possible. As soon as any multiplication can run (i.e., its inputs are available), it is executed. As soon as any result is produced, it is aggregated. That is, we would schedule computations

MODEL	WC SYSTEM	SYNCHRONOUS
CHAINMM	139	185.3
FFNN	50.2	76.9

Table 1: Execution time (in milliseconds) for execution in a work-conserving system (WC) system and a synchronous system. Configuration details can be found in Appendix F.

asynchronously, on-the-fly, so that resources such as network and GPU do not go unused. A dynamic scheduler that never willingly allows resources to sit idle and schedules them dynamically and asynchronously is referred to as a *work conserving dynamic scheduler* [27]. A work conserving (WC) system can have significant advantages compared to synchronous systems, as shown in Appendix G.

For a simple example of potential speedup, consider the execution of a chain of matrix multiplications and additions (CHAINMM) and a feedforward neural network (FFNN). Details of the computations are in Section 7. Running these on a GPU server using PyTorch compared to a WC system results in a 33% (CHAINMM) and a 53% (FFNN) increase in running time (see Table 1).

In this paper, we tackle a key problem associated with implementing a WC system for a multi-GPU server: producing the assignment of GPU kernel calls to devices. Device assignment problems are inherently difficult [2], especially in the non-deterministic context of WC systems. If a GPU kernel is slow to launch because of the prioritization of messages in a PCIe bus, for example—which is beyond the control of the system—another kernel may finish first and the entire execution order may be affected. One of the key considerations in assigning kernel calls to GPUs is the load balancing (computations evenly distributed across GPUs) of expensive tensor contractions. Whether an assignment is “load balanced” has an implicit temporal aspect—at every instant, all GPUs should have work to do, and none should be blocked, waiting for input. If the execution order is stochastic, it is difficult to define what it means for an assignment to be “load balanced” as the set of calls executed together may be different from run to run.

We propose a framework called DOPPLER that relies on a *dual policy* sequential decision scheme for device assignment in a WC system for multi-GPU computing. The first policy considers a partially-assigned dataflow graph and chooses the next vertex to assign. The second policy considers the graph and the selected vertex and assigns the vertex to a GPU.

The dual policy scheme allows for the separation of concerns: the first policy is tasked with traversing the vertices in an order that best approximates the non-deterministic flow of “time” through the graph, and the second policy is tasked with assigning a single vertex to ensure load balancing and to minimize communication.

DOPPLER uses a three-stage framework for training and deploying the dual policy. In Stage I (offline), the policies are trained in a supervised fashion to obey simple heuristics such as “put producers and consumers together”. In Stage II (offline), the policies are trained using reinforcement learning, where each assignment produced by the policies is “deployed” in a simulated WC system and the reward is computed using the simulated running time. In Stage III (online), the policies are deployed in a real-life WC system. DOPPLER enables these policies to be continuously refined using reinforcement learning, where the reward is computed using observed WC system running times.

Our contributions are the following: (1) We investigate the device assignment problem in a multi-GPU system under a work-conserving scheduler, aiming to enhance parallelization strategies during deployment; (2) We adopt a dual policy learning approach to first learn the approximated traversing order of nodes before assigning them to devices, enabling a better and an efficient learning process; (3) We propose DOPPLER, a three-stage training framework to improve scheduling efficiency on the fly by continuously training it during deployment, along with two pretraining stages to accelerate convergence in deployment; and (4) Our experiments show that DOPPLER achieves up to 62.5% lower execution times than the best baseline. DOPPLER achieves a further runtime reduction compared to a strong baseline (our own, special-purpose ENUMERATIVEOPTIMIZER) by up to 13.8%.

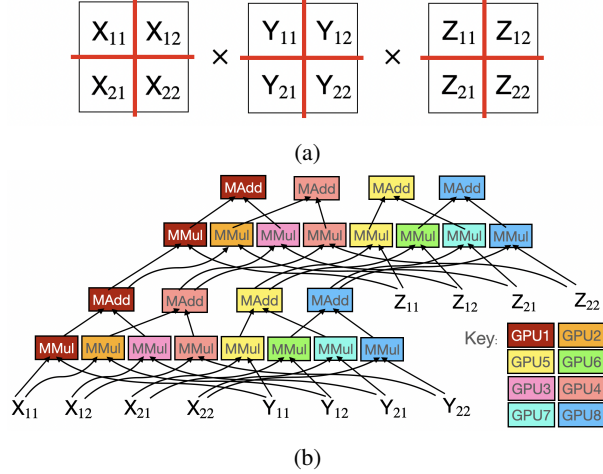


Figure 1: (a) A decomposition of a matrix multiplication chain. (b) A dataflow graph corresponding to the decomposed chain from (a). Colors show the mapping of computations to GPUs.

## 2 Device Assignment in a Work Conserving System

Formally, given a *dataflow graph*  $\mathcal{G} = \langle \mathcal{V}, \mathcal{E} \rangle$  with nodes  $\mathcal{V} = \{v_1, v_2, \dots, v_n\}$  representing computations, and edges  $\mathcal{E} = \{e_1, e_2, \dots, e_m\}$  representing data flows, as well as a set of devices  $\mathcal{D}$ , we aim to generate a *device assignment*  $A$  which is a mapping from  $\mathcal{V}$  to  $\mathcal{D}$ .  $A_v$  denotes the device associated with vertex  $v$  in  $A$ .  $A$  is chosen to minimize the execution time  $\text{ExecTime}(A)$ .

For an example dataflow graph, consider the matrix multiplication chain  $X \times Y \times Z$ . This can be decomposed or “exploded” to run on a server with eight GPUs by sharding each matrix four ways in Fig. 1a. Represented as a fine-grained dataflow graph, the sharded computation has eight submatrix multiplies associated with both of the two original multiplies, as well as four matrix additions to aggregate the results. The resulting graph, with an assignment to eight GPUs, is shown in Fig. 1b. This assignment may have a low execution time relative to lower-quality assignments, as (a)

the expensive matrix multiplications that will tend to run in parallel are load-balanced, and (b) communication is minimized by co-locating producers and consumers.

---

### Algorithm 1 ExecTime( $A$ )

---

```

% rdy[v, d] is true iff the result of vertex
% v is on device d; initially, nothing is ready
rdy[v, d] ← false ∀(v ∈ V, d ∈ D)
% except inputs: available everywhere
rdy[v, d] ← true ∀(v ∈ V, d ∈ D) s.t. (v', v) ∉ E
t ← 0 % exec begins at time 0
S ← {} % schedule is empty
while ∃(v ∈ V) s.t. rdy[v, A_v] = false do
  tasks ← EnumTasks(rdy, A, S)
  task ← ChooseTask(rdy, A, S, tasks)
  if task = null then
    % if no task is chosen, just wait
    ⟨t, task⟩ ∼ P(.|S, t) % which task done?
    S ← S + ⟨task, t, end⟩ % save completion
    rdy[vertex(task), device(task)] ← true
  else
    S ← S + ⟨task, t, beg⟩ % record initiation
  end if
end while
return t

```

---

## 3 Execution Time in a Work Conserving System

A key question is: how to define the execution time of an assignment  $\text{ExecTime}(A)$ ? It is difficult to give a simple, closed formula for  $\text{ExecTime}(A)$ , given the stochasticity of WC systems. As operations are issued dynamically, based on the state of the system, different runs of the same assignment can have very different execution times.

Algorithm 1 defines  $\text{ExecTime}(A)$ , which describes how an assignment  $A$  is executed in a WC system (the subroutine  $\text{EnumTasks}(rdy, A, S)$  in Algorithm 2 enumerates the tasks that can be taken in each step by the scheduler). The algorithm stochastically simulates the execution of the assignment  $A$  via a WC dynamic scheduler and returns the total execution time. It works by repeatedly asking the scheduler to choose the next task to schedule; when there is not a task that can be scheduled, the algorithm waits until an event is stochastically generated. In the algorithm, a *schedule*  $S$  is the complete list of events that have occurred up to  $t_{in}$ . An *event* is a  $(task, time, eventtype)$  triple, where *task* is either an execution result transfer between devices or an execute (exec) of a node on a device, *time* records when the transfer or exec event happens, and *eventtype* specifies the recorded time as either beg or end of an event.  $\text{EnumTasks}$  enumerates all transfer and exec tasks that are ready when  $\text{EnumTasks}$  is called.

Algorithm 1 has two key generic components that allow it to serve as a reasonable proxy or digital twin for a real-life scheduler, executed on real-life hardware. First, the distribution  $P(\langle t_{out}, a \rangle | S, t_{in})$

---

### Algorithm 2 EnumTasks( $rdy, A, S$ )

---

```

output ← {}
% get all potential transfers
for (v1, v2) ∈ E do
  if rdy[v1, A_v2] = false and rdy[v1, A_v1] =
  true and transfer(v1, A_v1, A_v2) ∉ S
  then
    Add transfer(v1, A_v1, A_v2) to output
  end if
end for
% get all potential ops to exec
for v2 ∈ V do
  if rdy[v1, A_v2] = true ∀v1 s.t. (v1, v2) ∈
  E and exec(v2, A_v2) ∉ S then
    Add exec(v2, A_v2) to output
  end if
end for
return output

```

---

---

**Algorithm 3** ASSIGN( $\text{SEL}_\theta, \text{PLC}_\theta$ )

---

```

 $A \leftarrow \{\}$ 
for  $t' \in \{1, \dots, m\}$  do
    Choose  $v \leftarrow \text{SEL}_\theta(A, \mathcal{G})$ 
    Choose  $d \leftarrow \text{PLC}_\theta(A, \mathcal{G}, v, \mathcal{D})$ 
    Add  $(v \rightarrow d)$  to  $A$ 
end for
return  $A$ 

```

---

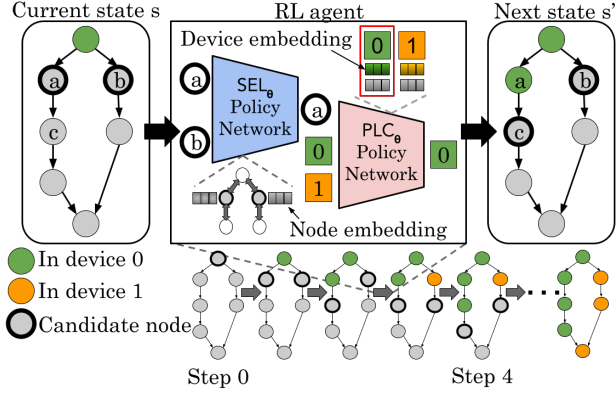


Figure 2: (Left) The ASSIGN algorithm, which sequentially produces an assignment  $A$  using  $\text{SEL}_\theta$  policy and placed using  $\text{PLC}_\theta$  policy. (Right) A graphical depiction of the algorithm’s implementation.

governs the “next completed task.” Given a schedule  $S$  and a current time  $t_{in}$ ,  $P$  is a joint distribution over the next task to complete and the time  $t_{out}$  at which this task completes. Second, the function `ChooseTask` encapsulates the underlying scheduling algorithm that is implemented by the WC system. It may choose any *task* from *tasks*. As described, it may operate depth-first (seeking to probe deeply into  $\mathcal{G}$ ), breadth-first, or may employ any other applicable strategy.

In practice, Algorithm 1 is implemented by either (a) a simulator where the distribution  $P(\langle t_{out}, a \rangle | S, t_{in})$  is realized by a model that takes into account factors such as the number of floating operations in the underlying operation (in the case of an operation such as a tensor contraction) or the number of bytes to be transferred (in the case of a GPU-to-GPU transfer), or (b) by actually deploying the assignment  $A$  in a real-life work-conserving system, and observing the running time. We use option (a) in Stage II of DOPPLER, and (b) in Stage III of DOPPLER (see Section 6).

#### 4 Problem Definition and a Solution via Reinforcement Learning

As there is no closed-form objective function, learning-by-doing is the most obvious approach for determining the optimal assignment  $A^*$ . Stages II and III of DOPPLER formulate choosing the assignment as a bandit problem.

Assume we choose assignment  $A$  at time tick  $t$  and obtain reward  $r_t \sim R_A$  where  $R_A$  is the reward distribution for  $A$  (in practice,  $r_t$  is sampled by invoking `ExecTime( $A$ )` and observing the runtime). Let  $R^* = R_{A^*}$  where  $A^* = \arg \max_A \mathbb{E}[R_A]$ . Our goal is to minimize the regret:

$$\rho = \sum_{t=1}^T (\mathbb{E}[R^*] - r_t) \quad (1)$$

This is a bandit problem with  $\mathcal{D}^{|\mathcal{V}|}$  arms. Our problem is not amenable to classic solutions because the number of arms is so large. For example, if we are producing an assignment for an 8-GPU server that is to execute a dataflow graph with 100 vertices, there are  $\approx 2^{300}$  possible assignments.

Fortunately, there is a combinatorial structure to the assignment problem that can allow us to deal with the very large set of possible assignments [9, 10]. Note that if two assignments  $A_1$  and  $A_2$  differ only in how a few vertices have been assigned to devices, it is likely that the two reward distributions  $R_{A_1}$  and  $R_{A_2}$  will be similar. Thus, it may be possible to systematically search the possible assignments.

The approach we propose builds the assignment at each time tick using a sequential process, controlled by two policies  $\text{SEL}_\theta$  and  $\text{PLC}_\theta$ . If we use  $\text{ASSIGN}(\text{SEL}_\theta, \text{PLC}_\theta)$  (Algorithm 3) as the mechanism for choosing the assignment  $A$  at each time tick  $t$  of the bandit problem of Equation 1, this process can be reformulated as an episodic Markov decision process (MDP) as shown in [32], where each episode executes  $\text{ASSIGN}(\text{SEL}_\theta, \text{PLC}_\theta)$  (shown in Figure 2) and a reward is obtained once the assignment is completed at the end of each episode. Therefore, any suitable reinforcement learning algorithm can be used to learn the policies  $\text{SEL}_\theta$  and  $\text{PLC}_\theta$ . In our implementation, we apply a graph neural network (GNN) along with message passing to encode graph  $\mathcal{G}$  and use a feedforward neural network for decoding actions for  $\text{SEL}_\theta$  and  $\text{PLC}_\theta$ . Details on GNN architectures are in Section 5.2.



## 5 DOPPLER Dual Policy Implementations

We describe our episodic Markov Decision Process formulation (Section 5.1), along with the graph neural network architectures that we used to implement the dual policy learned during DOPPLER training (Section 5.2) and an efficiency analysis of the GNN message-passing (Section 5.3).

### 5.1 Episodic MDP formulation

We formulate device assignment as an episodic Markov Decision Process (MDP)  $(\mathcal{S}, \mathcal{A}, H, \mathcal{P}, \mathcal{R})$  where  $\mathcal{P}$  is the transition function, and  $H$  is the horizon that equals the number of nodes in the graph.

**States** Each state  $s_h \in \mathcal{S}$  is a tuple  $(X_{\mathcal{G}}, \mathcal{C}_h, X_{\mathcal{D},h})$ , where  $X_{\mathcal{G}} = (X_{\mathcal{V}}, X_{\mathcal{E}})$  represents the static graph features including node and edge features such as bottom-level paths (i.e., to entry nodes), top-level (i.e., to exit nodes) paths, and communication costs.  $\mathcal{C}_h$  is the dynamic set of candidate nodes and  $\mathcal{C}_0$  is defined as the entry nodes in the graph. Finally,  $X_{\mathcal{D},h}$  represents the dynamic device features (e.g., total computing time and the end time for computations in each device). Details about the sets of features can be found in the Appendix D.

**Actions** At each time-step  $h$ , the agent takes an action  $a_h \in \mathcal{A}$  where  $a_h = (v_h, d_h)$ . Each action selects a node  $v_h$  and places it into device  $d_h$  using policies  $\text{SEL}_{\theta}$  and  $\text{PLC}_{\theta}$  as shown in Figure 2. Each episode is composed of  $|\mathcal{V}|$  iterations—i.e., one iteration per node in  $\mathcal{V}$ .

**Reward** We calculate rewards using the execution time  $R_{s_H} = (-1) * \text{ExecTime}(s_H)$  derived from either the real system or a simulator. The reward is computed at the end of each episode ( $h = H$ ), with intermediate rewards set to zero for efficiency. To enhance stability, we subtract a baseline reward equal to the average execution time observed across all previous episodes ( $\overline{R_{s_H}}$ ). The final reward is computed as  $r_H = R_{s_H} - \overline{R_{s_H}}$ .

### 5.2 Dual Policy Graph Neural Network Architectures

We will describe the policy networks for computing  $\text{SEL}_{\theta}$  and  $\text{PLC}_{\theta}$  in Algorithm 3. The symbol  $\theta$  is used here to emphasize that these functions have parameters that will be optimized as part of the training process. DOPPLER applies a Graph Neural Network (GNN) to encode node information in the dataflow graph. Our GNN is a message-passing neural network [18] that learns node representations for each node  $v$  via  $K$  successive iterations:

$$\mathbf{h}_v^{[k]} = \phi(\mathbf{h}_v^{[k-1]}, \bigoplus_{u \in N(v)} \psi(\mathbf{h}_u^{[k-1]}, \mathbf{h}_v^{[k-1]}, \mathbf{e}_{uv}))$$

where  $\mathbf{h}_v^{[k]}$  are representations learned at the  $k$ -th layer,  $\mathbf{h}_v^{[0]} = X_{\mathcal{V}}[v]$ ,  $\psi$  and  $\phi$  are functions,  $N(v)$  are the neighbors of  $v$ , and  $\bigoplus$  is a permutation-invariant operator. We will use  $\text{GNN}(\mathcal{G}, X_{\mathcal{G}}) = [\mathbf{h}_1^{[K]}; \mathbf{h}_2^{[K]}; \dots \mathbf{h}_n^{[K]}]$  to refer to the representations of all nodes in  $\mathcal{G}$ .

We also apply an  $L$ -layer feedforward neural network (FFNN) to encode node information:

$$\mathbf{x}_v^{[l]} = W^{[l]} \mathbf{x}_v^{[l-1]} + \mathbf{b}^{[l]}$$

where  $\mathbf{x}_v^{[l]}$  are representations at the  $l$ -th layer, and  $W^{[l]}$  and  $\mathbf{b}^{[l]}$  are weights and biases, respectively. Let  $\text{FFNN}(X) = [\mathbf{x}_1^{[L]}; \mathbf{x}_2^{[L]}; \dots \mathbf{x}_n^{[L]}]$  be the representations of all nodes in  $\mathcal{G}$  with  $\mathbf{x}_v^{[0]} = X[v]$ .

**Node policy network ( $\text{SEL}_{\theta}$ ):** Selects a node from the candidate set  $\mathcal{C}$  based on observed graph state  $X_{\mathcal{G}}$  using the  $\epsilon$ -greedy approach. Let  $b(v)$  and  $t(v)$  be the b-path and t-path for  $v$ , where a b-level (t-level) path for  $v$  is the longest path from  $v$  to an entry (exit) node in  $\mathcal{G}$ . We aggregate information from these critical paths via GNN embeddings  $H[u]$  for each node  $u$  along them. Nodes are selected according to probabilities estimated from a graph embedding matrix  $H_{\mathcal{G}}$ , which is a result of the concatenation of critical path ( $\mathbf{h}_{v,b}$  and  $\mathbf{h}_{v,t}$ ), GNN ( $H[v]$ ), and feature ( $Z[v]$ ) representations.

$$\begin{aligned} H &= \text{GNN}(\mathcal{G}, X_{\mathcal{G}}) & \mathbf{h}_{v,b} &= \sum_{u \in b(v)} H[u] & \mathbf{h}_{v,t} &= \sum_{u \in t(v)} H[u] \\ Z &= \text{FFNN}(X_{\mathcal{V}}) & \mathbf{h}_v &= [H[v] \parallel \mathbf{h}_{v,b} \parallel \mathbf{h}_{v,t} \parallel Z[v]] & H_{\mathcal{G}} &= [\mathbf{h}_1; \mathbf{h}_2; \dots \mathbf{h}_c] \\ H'_{\mathcal{G}} &= \text{LeakyReLU}(\text{FFNN}(H_{\mathcal{G}})) & Q_{\mathcal{G}}(v) &= \text{softmax}(\text{FFNN}(H'_{\mathcal{G}})) \end{aligned}$$

$$\text{SEL}_{\theta}(\mathcal{G}, X_{\mathcal{G}}) = \begin{cases} \arg \max_v Q_{\mathcal{G}}(v) & p = 1 - \epsilon \\ \text{random } v \in \mathcal{C} & p = \epsilon \end{cases}$$

where  $p$  is the probability of the event and  $\epsilon$  is a parameter.

**Device policy network (PLC $_{\theta}$ ):** Places a node  $v$  into one of the devices in  $\mathcal{D}$  based on the composed state observation  $(v, X_{\mathcal{D}}, X_{\mathcal{G}})$ . Devices are selected based on an embedding matrix  $H_{\mathcal{D}}$  for the set of devices generated by concatenating representations for the node ( $H[v]$ ), node features ( $Z[v]$ ), device features ( $Y[d]$ ), and for nodes already placed into the device ( $\mathbf{h}_d$ ).

$$\begin{aligned} H &= \text{GNN}(\mathcal{G}, X_{\mathcal{G}}) & \mathbf{h}_d &= \sum_{u: d_u=d} H[u] & Y &= \text{FFNN}(X_{\mathcal{D}}) \\ Z &= \text{FFNN}(X_{\mathcal{G}}) & \mathbf{h}_{v,d} &= [H[v] \parallel \mathbf{h}_d \parallel Y[d] \parallel Z[v]] & H_{\mathcal{D}} &= [\mathbf{h}_1; \mathbf{h}_2; \dots \mathbf{h}_m] \\ H'_{\mathcal{D}} &= \text{LeakyReLU}(\text{FFNN}(H_{\mathcal{D}})) & Q_{\mathcal{D}}(d) &= \text{softmax}(\text{FFNN}(H'_{\mathcal{D}})) \end{aligned}$$

$$\text{PLC}_{\theta}(v, \mathcal{D}, \mathcal{G}, X_{\mathcal{D}}, X_{\mathcal{G}}) = \begin{cases} \arg \max_d Q_{\mathcal{D}}(d) & p = 1 - \epsilon \\ \text{random } d \in \mathcal{D} & p = \epsilon \end{cases}$$

### 5.3 Efficient Message Passing Approximation

Implementing the MDP described in Section 5.1 requires performing message-passing on the dataflow graph  $\mathcal{G}$  when calling SEL $_{\theta}$  and PLC $_{\theta}$  policies at each MDP step  $h$ . We found this to be prohibitive for large graphs since we may apply up to  $8k \text{ episodes} \times 261 \text{ steps} = 2m \text{ steps}$  in our experiments. PLACETO (one of our baselines) suffers from this issue, being very inefficient during training as it performs one message-passing round per MDP step. Instead, we propose performing message passing on the graph only once per MDP episode and encoding updated assignment information at each step  $h$  in device  $X_{\mathcal{D},h}$  without message passing. We found empirically that this modification has a negligible impact over DOPPLER’s convergence but leads to a significant reduction in training time, especially for large neural networks (we show an ablation study in Appendix H.3).

## 6 DOPPLER: Cost-Effective Training

DOPPLER adopts a three-stage framework for training and deploying its dual policy (SEL $_{\theta}$  and PLC $_{\theta}$ ): (Stage I) imitation learning, (Stage II) simulation-based RL, and (Stage III) real-system RL (detailed figure shown in Appendix J). The idea is that imitation learning pre-training can speed up convergence in later RL stages by learning from an existing list scheduling heuristic. Moreover, two RL stages implement the “learning by doing” training concept for continuously learning the policies.

**Imitation Learning stage (Stage I).** We propose using imitation learning for teaching the dual policy to replicate the decisions of an existing heuristic (teacher) before deploying it to the real system. We apply the decisions of CRITICAL PATH [29] ( $a_{cp}$ ) and remove  $h$  for simplicity:

$$J(\theta) = \mathbb{E}_{a_{cp} \sim \Pi_{cp}(s), s \sim T(s', a), a \sim \Pi_{\theta}(s')} [\nabla_{\theta} \log \Pi_{\theta}(a_{cp}|s)] \quad (2)$$

**Simulation-based reinforcement learning stage (Stage II).** Even after pre-training with a teacher, we may have a policy that is too low-quality for deployment in the real system, where longer running times or slow convergence due to exploration may be unacceptable. Thus, we can train DOPPLER using a purely software-based simulator that implements Algorithm 1. The dual-policy networks are updated using the policy gradient method [41]. We maximize the following objective function:

$$J(\theta) = \mathbb{E}_{a \sim \Pi_{\theta}(s)} [\nabla_{\theta} (\log \Pi_{\theta}(a|s)) R(s, a)] \quad (3)$$

**Real-system reinforcement learning stage (Stage III).** Because the dual policy is of reasonably high quality before it is deployed in a user-facing environment, actual users need not suffer through long wait times due to low-quality assignments. Moreover, we envision that the dual policy can be continuously improved after its deployment in a real WC system with few iterations. Further, the reward signal for optimizing Equation 3 in this stage is obtained “for free” by observing real-life runtimes (ExecTime), so this continuous improvement of the assignments produced is possible with no additional cost. This is particularly convenient in Machine Learning as a Service (MLaaS) applications. Our experiments will show how this last stage works as fine-tuning for the dual-policy.

## 7 Experiments

We evaluate DOPPLER using dataflow graphs derived from multiple network architectures and compare our approach with the state-of-the-art methods. We focus on addressing the following

MODEL	1 GPU	4 GPUS					RUNTIME REDUCTION	
		CRIT. PATH	PLACETO	ENUMOPT.	DOPPLER-SIM	DOPPLER-SYS	BASELINE	ENUMOPT.
CHAINMM	439.9 $\pm$ 3.2	230.4 $\pm$ 4.3	137.1 $\pm$ 2.2	139 $\pm$ 10.0	<b>122.5</b> $\pm$ 4.0	123.4 $\pm$ 2.5	10.7%	11.9%
FFNN	148.5 $\pm$ 1.0	217.8 $\pm$ 11.3	126.3 $\pm$ 5.8	50.2 $\pm$ 2.5	49.9 $\pm$ 1.1	<b>47.4</b> $\pm$ 0.7	62.5%	5.6%
LLAMA-BLOCK	462.8 $\pm$ 7.6	230.9 $\pm$ 8.7	411.5 $\pm$ 19.7	172.7 $\pm$ 5.0	191.5 $\pm$ 5.97	<b>160.3</b> $\pm$ 4.30	30.6%	7.2%
LLAMA-LAYER	483.2 $\pm$ 8.2	292.6 $\pm$ 5.8	295.1 $\pm$ 7.0	174.8 $\pm$ 4.7	167 $\pm$ 3.4	<b>150.6</b> $\pm$ 4.2	48.5%	13.8%

Table 2: Real engine execution times (in milliseconds) for assignments identified by our approaches (ENUMOPT. and DOPPLER) compared against existing baselines. During training, both PLACETO and DOPPLER-SIM rely on a simulator to find good solutions, while others use a real system.

research questions: Q1: How does DOPPLER compare against alternative approaches in terms of execution time? Q2: What are the individual contributions of the  $SEL_\theta$  and  $PLC_\theta$  policies on DOPPLER’s performance? Q3: How can imitation learning, simulation-based RL, and real system RL be combined to improve DOPPLER’s training? Q4: How can DOPPLER’s execution time be interpreted based on the assignments it produces? Q5: Can DOPPLER be trained on one dataflow graph and be generalized to new graphs?

## 7.1 Experimental Setup

**Neural network architectures.** We test dataflow graphs from four types of neural network architectures in our experiments: a feed-forward neural network (FFNN), chain matrix multiplications (CHAINMM), a Llama transformer block (LLAMA-BLOCK), and a complete Llama transformer layer (LLAMA-LAYER). Further details can be found in Appendix C.

Model	4 GPUs		
	DOPPLER-SYS	DOPPLER-SEL	DOPPLER-PLC
ChainMM	123.4 $\pm$ 2.5	127.0 $\pm$ 0.8	<b>121.6</b> $\pm$ 0.7
FFNN	<b>47.4</b> $\pm$ 0.7	59.1 $\pm$ 7.6	63.2 $\pm$ 1.6
Llama-block	<b>160.3</b> $\pm$ 4.3	175.6 $\pm$ 4.1	172.9 $\pm$ 4.3
Llama-layer	<b>150.6</b> $\pm$ 4.2	161.7 $\pm$ 4.1	159.5 $\pm$ 4.9

Table 3: Real engine execution time (in milliseconds) of our approach (DOPPLER-SYS) against only applying  $SEL_\theta$  (DOPPLER-SEL) or only  $PLC_\theta$  (DOPPLER-PLC). The results show that both contribute to the performance improvements.

**GPU systems.** We compare the assignment approaches using 4 NVIDIA Tesla P100 GPUs and 16GB of memory each. We also consider a baseline using 1 GPU. Moreover, we did ablation studies on 1) 8GB out of 16GB restricted GPU memory, 2) 8 NVIDIA V100 GPUs with 32GB memory, and show results in Appendix I.

**Baselines.** We compare our approach against three baselines. CRITICAL PATH [29] is a popular (non-learning) heuristic for DAG device assignment. PLACETO [4] is a recent RL-based alternative that applies a single (device) policy and is trained using simulations (see ablation study on the simulator in Appendix H.1). ENUMERATIVEOPTIMIZER is a baseline we developed—it is our best effort at exploiting the structure of a sharded tensor computation to produce a high-quality assignment (described in detail in the Appendix A).

**Hyperparameters.** For RL-based methods, we run 4k episodes for CHAINMM and FFNN and 8k episodes for LLAMA-BLOCK and LLAMA-LAYER for all learning-based methods. We tried different learning rate schedules for each method (initial values  $\{1e-3, 1e-4, 1e-5\}$ ) and found that  $1e-3$  decreasing linearly to  $1e-6$  works best for PLACETO and  $1e-4$  linearly decreasing to  $1e-7$  works best for all versions of DOPPLER. We apply a 0.5 exploration rate linearly decreasing to 0.0 for PLACETO and 0.2 linearly decreasing to 0.0 for DOPPLER. An entropy weight of  $1e-2$  is applied for all RL methods. For CRITICAL PATH, we run 50 assignments and report the best execution time. The reported execution time (and standard deviation) using the real system is the average of 10 executions.

## 7.2 Results and Discussion

**Comparison between our solutions and existing alternatives (Q1).** Table 2 shows the comparison based on real system execution time and dataflow graphs for different neural network architectures on 4 GPUs. DOPPLER-SYS outperforms the alternatives in most of the settings and that DOPPLER-SIM is often the second best solution. For instance, DOPPLER-SYS achieves up to a 78.2% runtime reduction compared with CRITICAL PATH and up to a 62.5% runtime reduction compared with PLACETO. DOPPLER-SYS and DOPPLER-SIM also often outperform ENUMERATIVEOPTIMIZER by up to 13.8%. Further ablation studies on different training seeds are in Appendix H.2.

**Ablation study for select and place policies (Q2).** Table 3 shows an ablation study that separates the impact of the node policy and device policy networks on execution times. For the ablated methods, we replace our proposed policy with the strategy used by CRITICAL PATH. For DOPPLER-SEL, selected nodes are assigned to the device with the earliest start time. For DOPPLER-PLC, the nodes selected have the longest path to an exit node. We notice that combining both policy networks achieves the best results for the majority of tasks. Specifically, for ChainMM, DOPPLER-PLC marginally outperformed DOPPLER-SYS by a few milliseconds. However, for more complex models, combining both policy networks leads to performance improvements.

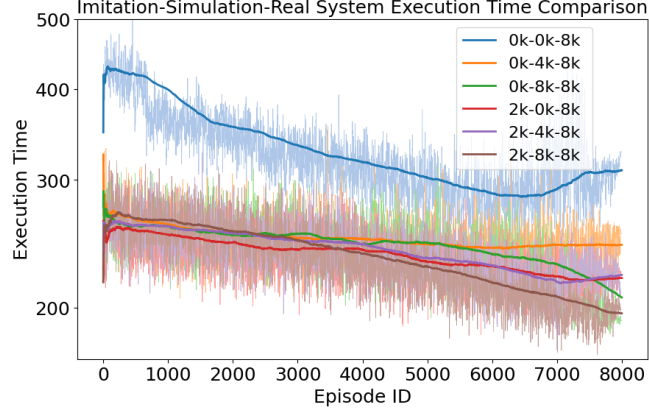


Figure 3: Real engine execution times (in milliseconds) for DOPPLER-SYS using different combinations of three training stages for the LLAMMA-LAYER dataflow graph.

**Improving training using imitation learning, simulation-based RL, and real system RL (Q3).** Figure 3 shows execution times for DOPPLER-SYS when trained using different combinations of imitation learning, simulations, and real system executions for the LLAMA-LAYER dataflow graph. As we hypothesized, training using the real system only leads to slower convergence due to the need for exploration starting from a poor initial model. Moreover, we find that training exclusively on the real system leads to unstable performance due to local optima. Imitation learning and simulations enable faster convergence and lower execution times. More ablation studies are conducted on pre-training PLACETO with imitation learning in Appendix H.4.

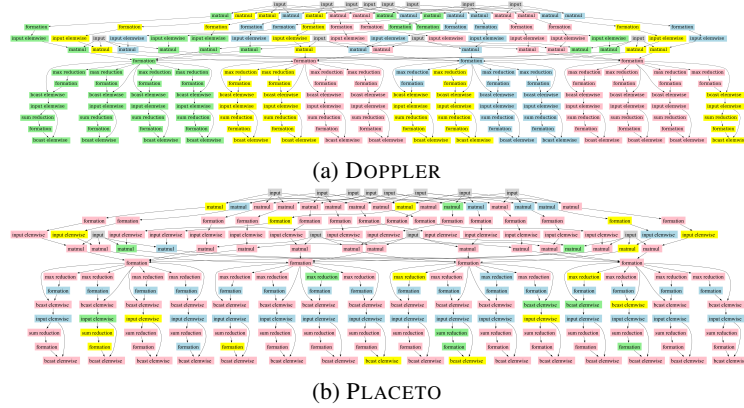


Figure 4: Assignments for FFNN found by DOPPLER and PLACETO. Colors show the mapping of computations to GPUs. DOPPLER is more effective at load balancing across GPUs.

**Comparing the assignments generated by PLACETO and DOPPLER-SYS (Q4).** Figure 4 compares the assignments produced by DOPPLER-SYS and PLACETO for the FFNN dataflow graph. We observe that DOPPLER outperforms PLACETO by minimizing GPU communications, resulting in a significant reduction in execution time. By further profiling how the assignments are scheduled in the system (see Appendix B for details), we can pinpoint specific advantages of our solution. DOPPLER schedules often enable overlapping communication and computation across GPUs, minimizing stalling and maximizing GPU utilization. These results demonstrate that our *dual policy* can be trained to maximize the benefits of a WC system. More device assignment visualizations and analyses can be found in Appendix E.

**Doppler’s transfer ability to new graphs (Q5).** We conduct a transfer learning study by applying simple architectures (FFNN and CHAINMM), to Llama-structured graphs. After 2K episodes of fine-tuning on the target model, DOPPLER adapts to the new architectures and outperforms all baselines in most cases. After 4K episodes of fine-tuning (less than half of the episodes in the original setups), DOPPLER finds assignments comparable to those obtained from full training on the target models.

		4 GPUs						
TRAIN MODEL	TARGET MODEL	ZERO-SHOT	2K-SHOT	4K-SHOT	DOPPLER-SYS	CRIT. PATH	PLACETO	ENUMOPT.
FFNN	LLAMA-BLOCK	251.0 $\pm$ 2.9	165.3 $\pm$ 4.1	<b>159.4</b> $\pm$ 4.8	<b>160.3</b> $\pm$ 4.3	230.9 $\pm$ 8.7	411.5 $\pm$ 19.7	172.7 $\pm$ 5.0
CHAINMM	LLAMA-BLOCK	242.3 $\pm$ 6.7	184.9 $\pm$ 4.3	<b>174.0</b> $\pm$ 4.4	<b>160.3</b> $\pm$ 4.3	230.9 $\pm$ 8.7	411.5 $\pm$ 19.7	172.7 $\pm$ 5.0
FFNN	LLAMA-LAYER	206.1 $\pm$ 4.5	158.2 $\pm$ 4.1	<b>155.8</b> $\pm$ 5.0	<b>150.6</b> $\pm$ 4.2	292.6 $\pm$ 5.8	295.1 $\pm$ 7.0	174.8 $\pm$ 4.7
CHAINMM	LLAMA-LAYER	338.2 $\pm$ 5.0	164.4 $\pm$ 3.3	<b>156.4</b> $\pm$ 4.4	<b>150.6</b> $\pm$ 4.2	292.6 $\pm$ 5.8	295.1 $\pm$ 7.0	174.8 $\pm$ 4.7

Table 4: Real engine execution times (in milliseconds) for assignments identified by DOPPLER under different few-shot settings (Zero-shot, 3k-shot, 4k-shot) compared against baselines. The results show that DOPPLER finds comparable results to full training (DOPPLER-SYS) in 4k-shot.

## 8 Related Works

**Classical Approaches for Device Placement and Scheduling.** List scheduling (LS) heuristics, such as CRITICAL PATH, decompose the problem of computing a schedule into a sequence of *select* and *place* steps [29]. DOPPLER can be seen as a neural LS heuristic that learns to *select* and *place* directly from observations using an MDP. Our experiments show that DOPPLER outperforms CRITICAL PATH. Graph partitioning [24, 26, 16, 22, 20, 23] can also be applied for device placement but previous work has shown that RL is a better alternative for the problem [36].

**Reinforcement Learning for Combinatorial Optimization.** Traditional algorithms for combinatorial optimization problems often rely on hand-crafted heuristics that involve sequentially constructing a solution. Recently, there has been a growing interest in applying RL (and deep learning more broadly) to learn heuristics for these problems [35]. For instance, [5] introduced a policy gradient method for the Traveling Salesman Problem (TSP). Subsequent studies extended RL to problems beyond TSP [25, 8, 13, 15, 33, 35, 37, 28, 13, 3, 34, 11, 31, 30, 19, 7]. Our work is unique in how it leverages the combinatorial structure with list scheduling heuristics and direct access to the target system during training to address the device assignment problem using RL.

**RL for Device Placement and Scheduling.** A sequence-to-sequence Recurrent Neural Network (RNN) for device placement trained with policy gradients was introduced in [36], showing that RL can outperform expert-designed heuristics [40]. PLACETO [4] replaced the RNN with a GNN and [38] combined RL and a Genetic Algorithm for joint placement and scheduling. However, [38] requires a substantial number of fitness evaluations per generation, which is not feasible during deployment. Moreover, each generation contains a considerable number of suboptimal execution assignments, leading to prolonged exploration time. [14] proposes a general end-to-end framework to optimize from the dataflow graph construction to device placement, and [21] improved node representations using a novel cosine phase position embedding scheme for device placement, which are complementary to the placement problem and can be incorporated into our approach.

## 9 Conclusions and Future Works

In this paper, we have considered the problem of assigning computations in a dataflow graph to devices to minimize execution time in a work-conserving system. In such an environment, it is crucial to assign computations effectively to ensure that the system never allows any resource to sit idle, waiting for an event such as a network transfer or a kernel call to finish. We have proposed DOPPLER, a dual-policy learning framework for learning device assignment in three stages. Some of the key innovations are (1) DOPPLER explicitly tries to learn an approximate node traversing order, to make the assignment problem easier, (2) DOPPLER adopts two pre-training stages using imitation learning and simulation-based learning to speed up policy convergence, and (3) DOPPLER continues dual-policy training during deployment, achieving a gradual reduction in execution time over time.

**Limitations & Societal Impact** The dual policy is inexpensive to train on the evaluated dataflow graphs; however, its training time grows with the size of the graph (see Appendix K). We only evaluated DOPPLER’s transfer ability from CHAINMM and FFNN to LLAMA-BLOCK and LLAMA-LAYER on the same hardware configuration. Future work could explore DOPPLER’s transfer capability across other dataflow graphs with different hardware configurations. This paper aims to advance the field of ML by improving efficiency in executing computations in multi-GPU systems. Our work has significant potential societal benefits on reducing power consumption and carbon footprint and expanding access to deep learning technologies through optimized multi-GPU utilization.

## References

- [1] Martín Abadi, Paul Barham, Jianmin Chen, Zhifeng Chen, Andy Davis, Jeffrey Dean, Matthieu Devin, Sanjay Ghemawat, Geoffrey Irving, Michael Isard, et al. {TensorFlow}: a system for {Large-Scale} machine learning. In *12th USENIX symposium on operating systems design and implementation (OSDI 16)*, pages 265–283, 2016.
- [2] Mohammed Abdullahi and Md Asri Ngadi. Hybrid symbiotic organisms search optimization algorithm for scheduling of tasks on cloud computing environment. *PloS one*, 11(6):e0158229, 2016.
- [3] Kenshin Abe, Zijian Xu, Issei Sato, and Masashi Sugiyama. Solving np-hard problems on graphs with extended alphago zero. *arXiv preprint arXiv:1905.11623*, 2019.
- [4] Ravichandra Addanki, Shaileshh Bojja Venkatakrishnan, Shreyan Gupta, Hongzi Mao, and Mohammad Alizadeh. Placeto: Learning generalizable device placement algorithms for distributed machine learning. *arXiv preprint arXiv:1906.08879*, 2019.
- [5] Irwan Bello, Hieu Pham, Quoc V Le, Mohammad Norouzi, and Samy Bengio. Neural combinatorial optimization with reinforcement learning. *arXiv preprint arXiv:1611.09940*, 2016.
- [6] Daniel Bourgeois, Zhimin Ding, Dimitrije Jankov, Jiehui Li, Mahmoud Sleem, Yuxin Tang, Jiawen Yao, Xinyu Yao, and Chris Jermaine. EinDecomp: Decomposition of declaratively-specified machine learning and numerical computations for parallel execution. *Proceedings of the VLDB Endowment*, 18(7):2240–2253, 2025.
- [7] Qingpeng Cai, Will Hang, Azalia Mirhoseini, George Tucker, Jingtao Wang, and Wei Wei. Reinforcement learning driven heuristic optimization. *arXiv preprint arXiv:1906.06639*, 2019.
- [8] Quentin Cappart, Emmanuel Goutierre, David Bergman, and Louis-Martin Rousseau. Improving optimization bounds using machine learning: Decision diagrams meet deep reinforcement learning. In *Proceedings of the AAAI Conference on Artificial Intelligence*, volume 33, pages 1443–1451, 2019.
- [9] Nicolo Cesa-Bianchi and Gábor Lugosi. Combinatorial bandits. *Journal of Computer and System Sciences*, 78(5):1404–1422, 2012.
- [10] Wei Chen, Yajun Wang, and Yang Yuan. Combinatorial multi-armed bandit: General framework and applications. In *International conference on machine learning*, pages 151–159. PMLR, 2013.
- [11] Xinyun Chen and Yuandong Tian. Learning to perform local rewriting for combinatorial optimization. *Advances in neural information processing systems*, 32, 2019.
- [12] Zhimin Ding, Jiawen Yao, Brianna Barrow, Tania Lorido Botran, Christopher Jermaine, Yuxin Tang, Jiehui Li, Xinyu Yao, Sleem Mahmoud Abdelghafar, and Daniel Bourgeois. Turnip: A "nondeterministic" gpu runtime with cpu ram offload. *arXiv preprint arXiv:2405.16283*, 2024.
- [13] Iddo Drori, Anant Kharkar, William R Sickinger, Brandon Kates, Qiang Ma, Suwen Ge, Eden Dolev, Brenda Dietrich, David P Williamson, and Madeleine Udell. Learning to solve combinatorial optimization problems on real-world graphs in linear time. In *2020 19th IEEE International Conference on Machine Learning and Applications (ICMLA)*, pages 19–24. IEEE, 2020.
- [14] Shukai Duan, Heng Ping, Nikos Kanakaris, Xiongye Xiao, Peiyu Zhang, Panagiotis Kyriakis, Nesreen K Ahmed, Guixiang Ma, Mihai Capota, Shahin Nazarian, et al. A structure-aware framework for learning device placements on computation graphs. *arXiv preprint arXiv:2405.14185*, 2024.
- [15] Patrick Emami and Sanjay Ranka. Learning permutations with sinkhorn policy gradient. *arXiv preprint arXiv:1805.07010*, 2018.
- [16] Charles M Fiduccia and Robert M Mattheyses. A linear-time heuristic for improving network partitions. In *Papers on Twenty-five years of electronic design automation*, pages 241–247. 1988.

- [17] Roy Frostig, Matthew James Johnson, and Chris Leary. Compiling machine learning programs via high-level tracing. *Systems for Machine Learning*, 4(9), 2018.
- [18] Justin Gilmer, Samuel S Schoenholz, Patrick F Riley, Oriol Vinyals, and George E Dahl. Neural message passing for quantum chemistry. In *International conference on machine learning*, pages 1263–1272. PMLR, 2017.
- [19] Shenshen Gu and Yue Yang. A deep learning algorithm for the max-cut problem based on pointer network structure with supervised learning and reinforcement learning strategies. *Mathematics*, 8(2):298, 2020.
- [20] Lars Hagen and Andrew B Kahng. New spectral methods for ratio cut partitioning and clustering. *IEEE transactions on computer-aided design of integrated circuits and systems*, 11(9):1074–1085, 1992.
- [21] Meng Han, Yan Zeng, Jilin Zhang, Yongjian Ren, Meiting Xue, and Mingyao Zhou. A novel device placement approach based on position-aware subgraph neural networks. *Neurocomputing*, 582:127501, 2024.
- [22] David S Johnson, Cecilia R Aragon, Lyle A McGeoch, and Catherine Schevon. Optimization by simulated annealing: An experimental evaluation; part i, graph partitioning. *Operations research*, 37(6):865–892, 1989.
- [23] George Karypis. Metis: Unstructured graph partitioning and sparse matrix ordering system. *Technical report*, 1997.
- [24] Brian W Kernighan and Shen Lin. An efficient heuristic procedure for partitioning graphs. *The Bell system technical journal*, 49(2):291–307, 1970.
- [25] Elias Khalil, Hanjun Dai, Yuyu Zhang, Bistra Dilkina, and Le Song. Learning combinatorial optimization algorithms over graphs. *Advances in neural information processing systems*, 30, 2017.
- [26] Scott Kirkpatrick, C Daniel Gelatt Jr, and Mario P Vecchi. Optimization by simulated annealing. *science*, 220(4598):671–680, 1983.
- [27] Leonard Kleinrock. A conservation law for a wide class of queueing disciplines. *Naval Research Logistics Quarterly*, 12(2):181–192, 1965.
- [28] Wouter Kool, Herke Van Hoof, and Max Welling. Attention, learn to solve routing problems! *arXiv preprint arXiv:1803.08475*, 2018.
- [29] Yu-Kwong Kwok and Ishfaq Ahmad. Static scheduling algorithms for allocating directed task graphs to multiprocessors. *ACM Computing Surveys (CSUR)*, 31(4):406–471, 1999.
- [30] Alexandre Laterre, Yunguan Fu, Mohamed Khalil Jabri, Alain-Sam Cohen, David Kas, Karl Hajjar, Torbjorn S Dahl, Amine Kerkeni, and Karim Beguir. Ranked reward: Enabling self-play reinforcement learning for combinatorial optimization. *arXiv preprint arXiv:1807.01672*, 2018.
- [31] Dongda Li, Changwei Ren, Zhaoquan Gu, Yuexuan Wang, and Francis Lau. Solving packing problems by conditional query learning. 2020.
- [32] Xutong Liu, Siwei Wang, Jinhang Zuo, Han Zhong, Xuchuang Wang, Zhiyong Wang, Shuai Li, Mohammad Hajiesmaili, John Lui, and Wei Chen. Combinatorial multivariate multi-armed bandits with applications to episodic reinforcement learning and beyond. *arXiv preprint arXiv:2406.01386*, 2024.
- [33] Hao Lu, Xingwen Zhang, and Shuang Yang. A learning-based iterative method for solving vehicle routing problems. In *International conference on learning representations*, 2019.
- [34] Sahil Manchanda, Akash Mittal, Anuj Dhawan, Sourav Medya, Sayan Ranu, and Ambuj Singh. Learning heuristics over large graphs via deep reinforcement learning. *arXiv preprint arXiv:1903.03332*, 2019.



- [35] Nina Mazyavkina, Sergey Sviridov, Sergei Ivanov, and Evgeny Burnaev. Reinforcement learning for combinatorial optimization: A survey. *Computers & Operations Research*, 134:105400, 2021.
- [36] Azalia Mirhoseini, Hieu Pham, Quoc V Le, Benoit Steiner, Rasmus Larsen, Yuefeng Zhou, Naveen Kumar, Mohammad Norouzi, Samy Bengio, and Jeff Dean. Device placement optimization with reinforcement learning. In *International conference on machine learning*, pages 2430–2439. PMLR, 2017.
- [37] Mohammadreza Nazari, Afshin Oroojlooy, Lawrence Snyder, and Martin Takác. Reinforcement learning for solving the vehicle routing problem. *Advances in neural information processing systems*, 31, 2018.
- [38] Aditya Paliwal, Felix Gimeno, Vinod Nair, Yujia Li, Miles Lubin, Pushmeet Kohli, and Oriol Vinyals. Reinforced genetic algorithm learning for optimizing computation graphs. *arXiv preprint arXiv:1905.02494*, 2019.
- [39] Adam Paszke, Sam Gross, Francisco Massa, Adam Lerer, James Bradbury, Gregory Chanan, Trevor Killeen, Zeming Lin, Natalia Gimelshein, Luca Antiga, et al. Pytorch: An imperative style, high-performance deep learning library. *Advances in neural information processing systems*, 32, 2019.
- [40] François Pellegrini. A parallelisable multi-level banded diffusion scheme for computing balanced partitions with smooth boundaries. In *Euro-Par 2007 Parallel Processing: 13th International Euro-Par Conference, Rennes, France, August 28-31, 2007. Proceedings 13*, pages 195–204. Springer, 2007.
- [41] Richard S Sutton, David McAllester, Satinder Singh, and Yishay Mansour. Policy gradient methods for reinforcement learning with function approximation. *Advances in neural information processing systems*, 12, 1999.
- [42] Vignesh Yaadav. Exploring and building the llama 3 architecture: A deep dive into components, coding, and inference techniques, 2024.
- [43] Lianmin Zheng, Zhuohan Li, Hao Zhang, Yonghao Zhuang, Zhifeng Chen, Yanping Huang, Yida Wang, Yuanzhong Xu, Danyang Zhuo, Eric P Xing, et al. Alpa: Automating inter-and {Intra-Operator} parallelism for distributed deep learning. In *16th USENIX Symposium on Operating Systems Design and Implementation (OSDI 22)*, pages 559–578, 2022.

## A Enumerative Assignment Algorithm (Algorithm 4)

In this section, we describe our enumerative assignment algorithm, which uses a level-by-level, exhaustive enumeration in an attempt to find an assignment  $A$  for the vertices in a graph  $\mathcal{G}$  to minimize  $\text{ExecTime}(A)$ . This algorithm uses a greedy approach that first groups vertices based on the graph structure and then attempts a subset of possible assignments for the operations within each group and selects the assignment with the minimum estimated cost.

This algorithm requires that the vertices in the graph  $\mathcal{G}$  have been organized into a list of “meta-ops” called  $M$ . As our input dataflow graph has been created by sharding a compute graph using a framework such as Alpa [43], each operation in the input dataflow graph  $\mathcal{G}$  is descended from some operation that has been sharded. For example, consider Figure 1. All of the eight `MMu1` ops at the lowest level of the graph, as well as the four `MAdd` ops at the next level were created by sharding  $X \times Y$ . We group all of these twelve operations and term them a “meta-op”. Further, we can topologically order these meta-ops so that if  $m_1$  comes before  $m_2$  in  $M$ , it means that none of the vertices in  $m_2$  can be reached from some vertex in  $m_1$  by traversing  $\mathcal{E}$ .

Note that each meta-op has two subsets—one of which may be empty: a set of computationally expensive operations (such as the `MMu1` ops) that result directly from sharding the original operation, and a set of less expensive operations needed to aggregate and/or recompose the results of the first set of operations. For a meta-op  $m$ , we call these  $m.\text{shardOps}$  and  $m.\text{reduceOps}$ . Note that the original operation is always sharded so that if there are  $n$  devices, there are  $n$  items in  $m.\text{shardOps}$ , and load-balancing of these shards is crucial. Thus, our tactic will be to always partition  $m.\text{shardOps}$  across the  $n$  devices, and never assign two operations in  $m.\text{shardOps}$  to the same device. Likewise, if the meta-op is sharded into  $n$  there will always be at most  $n$  items in  $m.\text{reduceOps}$ . Therefore, we always partition them across (possibly a subset of) the devices.

Given this, our algorithm “EnumerativeOptimizer” proceeds through the list  $M$  of meta-ops in order. For each  $m$ , it exhaustively tries all assignments of  $m.\text{shardOps}$ . Each assignment is costed by computing the time required to transfer all of the items in  $m.\text{shardOps}$  to where they will be consumed. These times are estimated using statistics gathered by testing transfers on the actual hardware. Once  $m.\text{shardOps}$  is placed, then  $m.\text{reduceOps}$  is placed, using the same cost model. Because of the ordering of the meta-ops in  $M$ , and because we process  $m.\text{shardOps}$  before  $m.\text{reduceOps}$ , we always know the assignment of the input to  $m.\text{shardOps}$  or  $m.\text{reduceOps}$  before we place it, and so it is easy to compute the cost.

This algorithm is greedy in the sense that it processes meta-ops one at a time, from start to finish, using the topological ordering. Thus, if the cost model is correct, it will be optimal only as long as each  $m.\text{shardOps}$  and  $m.\text{reduceOps}$  is run in lock-step, with a barrier before each set is executed. Obviously, this is not the case in reality with a dynamic scheduler, but one might expect the algorithm to produce a good assignment in practice.

## B System Implementation

The underlying system runtime [6, 12] that executes our graphs is written in C++. The dataflow graph  $\mathcal{G}$  is executed asynchronously by a single-threaded event loop whose job is to monitor when the dependencies implicit in the graph are satisfied. When the inputs to a vertex are found to be available, the event loop checks whether the resources necessary to execute the vertex are also available (a “resource” may be an open GPU stream or an open communication channel). If resources are available, the event loop may choose to execute the vertex. We use the term “event loop” because the loop asks the necessary resources to execute the vertices in  $\mathcal{G}$  in response to “events.” An event occurs whenever a graph dependency is satisfied, or when a previously used resource becomes available. The main event loop is notified of this via an asynchronous callback. In our implementation, we use CUDA version 11.8.0 and cuTensor version 2.0.1.

---

**Algorithm 4** EnumerativeOptimizer

---

**Input:** Sorted list of meta-ops  $M$  containing all vertices in  $\mathcal{G}$   
**Output:** Assignment  $A$   
 $A \leftarrow \langle \rangle$  % assignment is empty  
% loop thru meta-ops  
**for**  $m \in M$  **do**  
    % First deal with the shared op  
     $A \leftarrow \text{getBestAssign}(m.\text{shardOps}, A)$   
    % now place the reductions  
     $A \leftarrow \text{getBestAssign}(m.\text{reduceOps}, A)$   
**end for**  
return  $A$

% computes the best assignment for a set of vertices that are expected to run in parallel on all devices  
**subroutine**  $\text{getBestAssign}(\text{vertices}, A)$   
 $\text{bestCost} \leftarrow \infty; \text{bestAssign} \leftarrow \text{null}$   
% loop through all possible device assignments  
**for**  $D \in \text{allPerms}(\mathcal{D})$  **do**  
     $\text{whichDev} \leftarrow 0; \text{cost} \leftarrow 0$   
    % loop through the ops created by sharding this meta-op  
    **for**  $v \in \text{vertices}$  **do**  
        % loop through inputs to this op and add network cost  
        **for**  $v_1 \in \mathcal{V}$  s.t.  $(v_1, v) \in \mathcal{E}$  **do**  
             $\text{cost} \leftarrow \text{cost} + \text{getNetworkTime}(v_1, a_{v_1}, D_{\text{whichDev}})$   
        **end for**  
         $\text{whichDev} \leftarrow \text{whichDev} + 1$   
    **end for**  
    **if**  $\text{cost} < \text{bestCost}$  **then**  
         $\text{bestCost} \leftarrow \text{cost}$   
         $\text{bestAssign} \leftarrow D$   
    **end if**  
**end for**  
% we have the best assignment for this meta op, so record it  
 $\text{whichDev} \leftarrow 0$   
**for**  $v \in \text{vertices}$  **do**  
     $a_v \leftarrow D_{\text{whichDev}}$   
    append  $a_v$  to  $A$   
     $\text{whichDev} \leftarrow \text{whichDev} + 1$   
**end for**  
return  $A$

---

## C Computation Graphs Used in the Experiments

### C.1 ChainMM

- **Input matrices:**  $A, B, C, D, E \in \mathbb{R}^{10000 \times 10000}$
- **Neural Network Function:**  $(A \times B) + (C \times (D \times E))$
- **Number of nodes in the graph:** 112

### C.2 FFNN

- **Input batch matrix:**  $X \in \mathbb{R}^{2^{15} \times 2^5}$
- **First layer weight matrix:**  $W^{(1)} \in \mathbb{R}^{2^5 \times 2^{16}}$
- **First hidden layer bias vector:**  $b^{(1)} \in \mathbb{R}^{2^{16}}$
- **Output layer weight matrix:**  $W^{(2)} \in \mathbb{R}^{2^{16} \times 2^5}$

- **Output layer bias vector:**  $b^{(2)} \in \mathbb{R}^{2^5}$
- **Number of nodes in the graph:** 192
- $\text{ReLU}(\cdot)$  denotes the element-wise rectified linear activation function.
- $\text{Softmax}(\cdot)$  denotes the softmax activation function applied over the output dimensions to obtain class probabilities.
- **Neural Network Function:**
  - **Hidden layer computation:**  $H = \text{ReLU}(X \cdot W^{(1)} + b^{(1)})$  Here,  $H \in \mathbb{R}^{2^{15} \times 2^{16}}$ .
  - **Output layer computation:**  $Y = \text{Softmax}(H \cdot W^{(2)} + b^{(2)})$  Here,  $Y \in \mathbb{R}^{2^{15} \times 2^5}$  represents the output probabilities after applying softmax.

### C.3 Llama-block and Llama-layer

Hyperparameters for llama structure include:

- **Number of parameters:** 7B
- **Max sequence length:** 4096
- **Embedding dimension:** 4096
- **Number of tokens:** 32000
- **Batch size:** 1
- **Number of layers:** 1
- **Number of nodes in the graph:** 215
- **Neural Network Function:** Figure 5 shows the structure of Llama represented in the computation graphs Llama-block and Llama-layer.

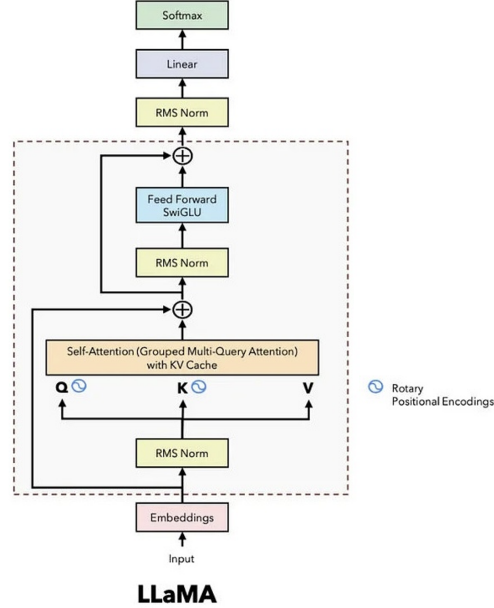


Figure 5: Llama-block and Llama-layer architecture. Figure from [42]

## D Graph Features $X_G$ and Device Features $X_D$ .

Given a computation graph  $\mathcal{G} = (\mathcal{V}, \mathcal{E})$  with  $\mathcal{V} = \{v_1, v_2, \dots, v_n\}$  and  $\mathcal{E} = \{e_1, e_2, \dots, e_m\}$ , we define the following:

- **Computation cost for  $v$ .** We use floating point operations per second of  $v$  as the computation cost.
- **Communication cost for  $e_{i,j} = (v_i, v_j)$ .** The number of bytes for the output tensor of  $v_i$  times a communication factor. In our case, we set the communication factor equal to 4. We benchmark the execution time of a simulator versus the real execution engine. We tried the values communication factor from 1 to 10 and found 4 to be the closest for the simulator with respect to the real execution engine.

### D.1 Static Graph Features $X_G$

The graph features matrix  $X_G$  is a  $n \times 5$  matrix where each row contains the following five features:

- **Computation cost for  $v_j$ .**
- **Sum of communication cost from predecessor nodes to  $v_j$ .** The sum of communication cost for all  $e_{i,j}$  such that  $(v_i, v_j) \in \mathcal{E}$ .
- **Sum of communication cost from  $v_j$  to descendant nodes.** The sum of communication cost for all  $e_{j,k}$  such that  $(v_j, v_k) \in \mathcal{E}$ .
- **t-level cost of  $v_j$ .** The sum of all computation costs and communication costs on a t-level path for  $v_j$ . A t-level path is defined in Section 5.2.
- **b-level cost of  $v_j$ .** The sum of all computation costs and communication costs on a b-level path for  $v_j$ . A b-level path is defined in Section 5.2.

### D.2 Dynamic Device Features $X_D$ for device $d$ at timestep $t$ given node $v$

The device features matrix  $X_D$  is a  $|D| \times 5$  matrix where each row contains the following five features:

- **Total node computation cost.** Sum of the computation costs for all the nodes that have been assigned to device  $d$  at timestep  $t$ .
- **Total predecessor nodes computation cost.** Sum of computation costs for all predecessor nodes of target node  $v$  at timestep  $t$  that are currently being assigned on device  $d$ .
- **Min start time of all input.** Earliest time to start execute a predecessor node of  $v$  on each device  $d$  at timestep  $t$ .
- **Max end time of all input.** Latest time for all predecessor nodes of  $v$  to finish on each device  $d$  at timestep  $t$ .
- **Earliest start time to compute  $v$ .** Earliest time for a device  $d$  to finish receiving inputs on  $d$  and start execute  $v$ .

## E More Device Assignment Analysis and Visualizations

### E.1 Computation node details

- **input:** input tensors
- **matmul:** matrix multiplications on two matrices
- **input elemwise:** elementwise operations(eg. ReLU) on an input tensor.
- **straight elemwise:** elementwise operations(eg. ReLU) with two inputs having the same dimensions.
- **bcast elemwise:** takes two inputs of different shapes (eg. a matrix and a vector) performing an elementwise operation(eg. ReLU) with one element of the vector on an entire row of the matrix.
- **max reduction:** reduce one dimension by finding max.
- **min reduction:** reduce one dimension by finding min.
- **sum reduction:** reduce one dimension by finding the sum along that dimension.
- **product reduction:** reduce one dimension by finding the product along that dimension.
- **formation:** a placeholder operation that forces aggregations in joinAgg groups to form a single tensor.
- **complexer:** a conversion between floats and complex tensors.
- **fill:** an operation to create tensors with all the same scalar, or to assign all lower or upper diagonal elements with provided scalar values.
- **squeezer:** adding or removing singleton dimensions of a tensor.
- **selec.:** an operation to copy a subset of several input tensors into an output tensor—a generalization of tensor subset and tensor concatenation.

## E.2 Assignment profiling

This section examines the performance results from Table 2, where the DOPPLER algorithm achieved a lower runtime compared to CRITICAL PATH, PLACETO and the expert-designed ENUMERATIVEOPTIMIZER.

During the development of the ENUMERATIVEOPTIMIZER algorithm, it became clear that for meta-ops (described in Appendix A) containing many computations, the devices should be fully utilized and load-balanced. *Put more succinctly, it is expected that good assignments should minimize data transfers while maximizing computational resource utilization.*

**CHAINMM:** The assignments in Figure 6 for DOPPLER show all four devices used whereas for ENUMERATIVEOPTIMIZER, Figure 7, only two of the devices are used for the latter computations. The corresponding device utilization plots are shown in Figure 8 and Figure 9, respectively. It appears that, indeed, ENUMERATIVEOPTIMIZER does not fully utilize available compute resources towards the end of the computation. On the contrary, DOPPLER does well from the beginning to the end as shown in Figure 6.

**FFNN:** The assignments for FFNN with DOPPLER and PLACETO are shown in Figure 4; the corresponding device utilization are shown in Figure 10 and Figure 11. In the DOPPLER assignments, subsequent vertices typically share the same device assignment. In turn, this should lead to a lower amount of data transfer. For the PLACETO assignments, however, subsequent vertices do not tend to have the same device assignment, possibly leading to a large amount of data transfer. In the device utilization figures, this is indeed borne out, where the PLACETO execution is three times slower, with most time spent on data transfers across GPUs.

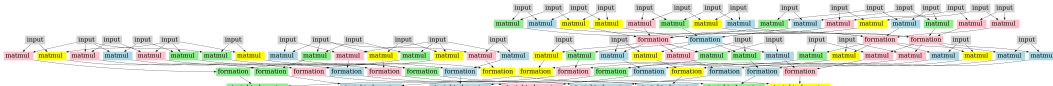


Figure 6: Assignment found by Doppler for ChainMM

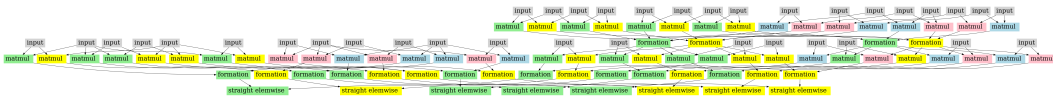


Figure 7: Assignment found by EnumerativeOptimizer for ChainMM



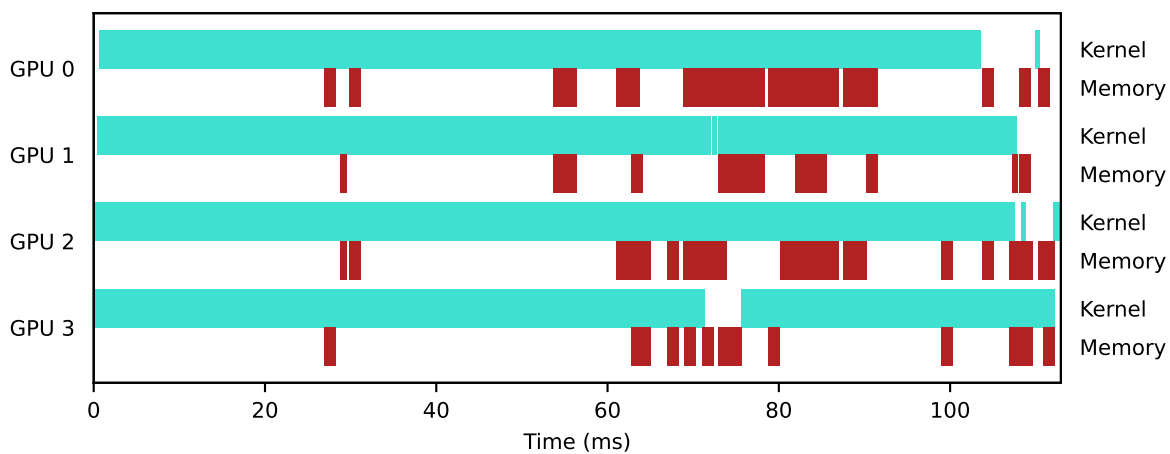


Figure 8: Device and transfer utilization for DOPPLER, CHAINMM.

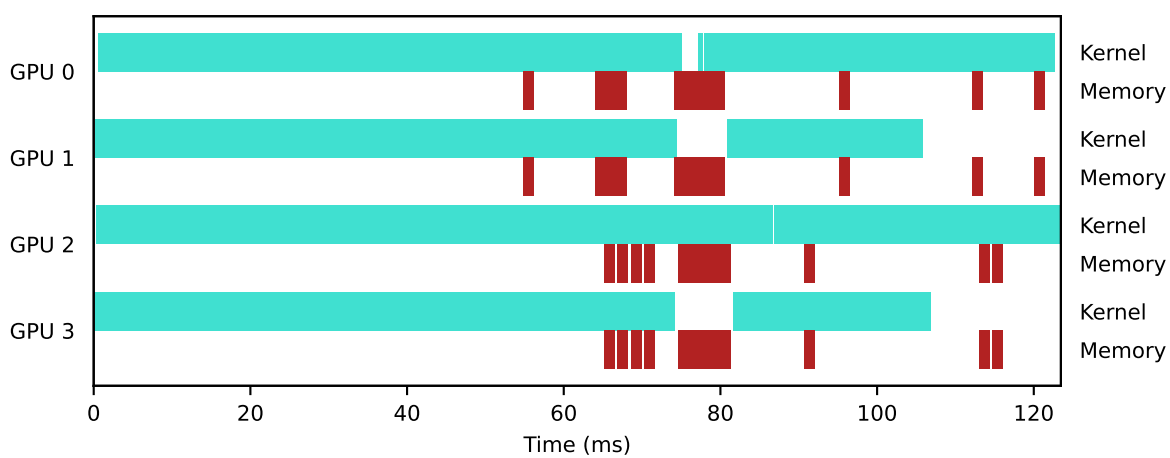


Figure 9: Device and transfer utilization for ENUMERATIVEOPTIMIZER, CHAINMM.

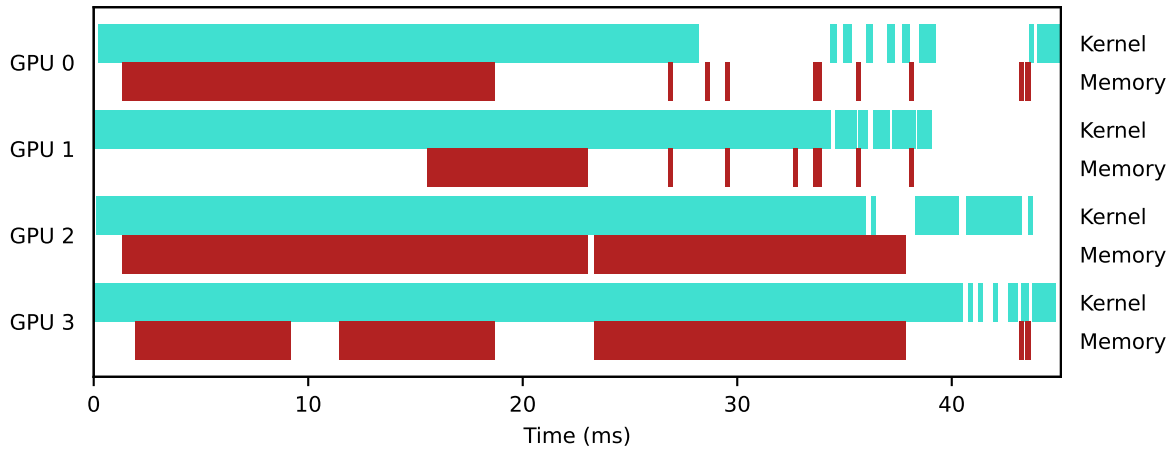


Figure 10: Device and transfer utilization for DOPPLER, FFNN.

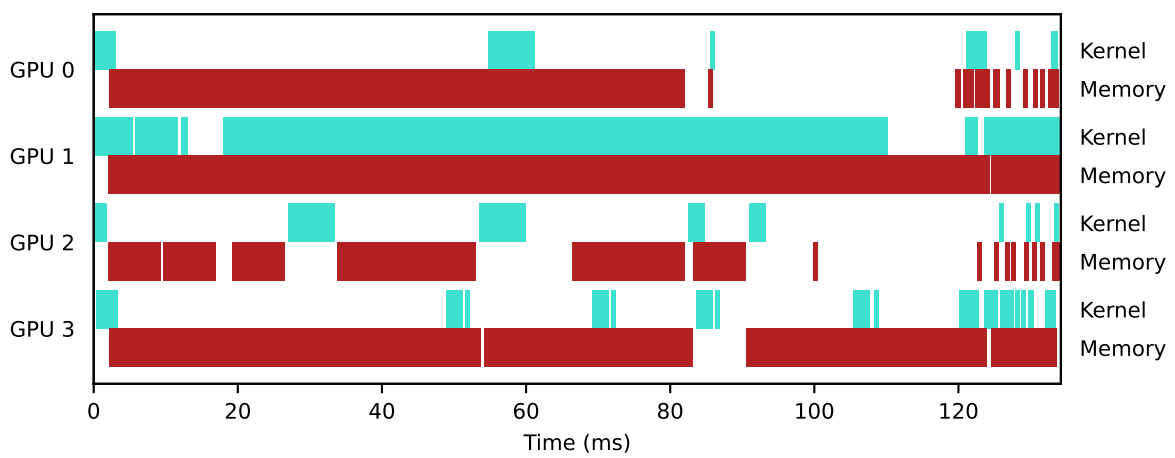


Figure 11: Device and transfer utilization for PLACETO, FFNN.

### E.3 Llama-block Assignment Analysis

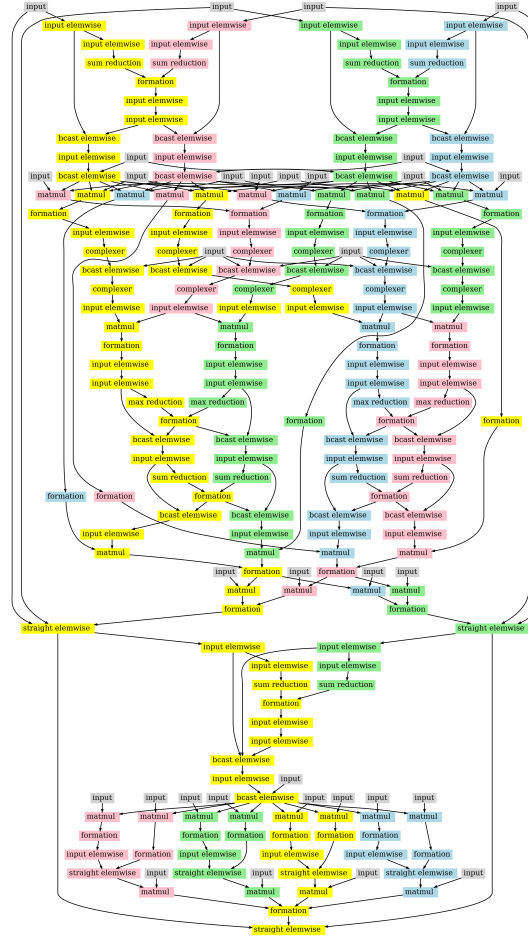


Figure 12: Assignment found by DOPPLER for LLAMA-BLOCK

The experiments demonstrate DOPPLER’s capability to efficiently achieve load balancing in a distributed computing environment, particularly when multiple GPUs are utilized for computation. Across varied workloads, we observed that DOPPLER distributes workloads more evenly across available GPUs, ensuring that no single device is over-utilized while others remain under-utilized. Additionally, further analysis has provided deeper insights into DOPPLER’s ability to make better assignment decisions, ensuring that computational tasks are assigned in a way that maximizes efficiency and minimizes stalling. This improves system performance and enables more effective resource utilization in distributed GPU computing environments as shown in Figure 12.

For instance, when executing a single LLAMA-BLOCK, PLACETO demonstrates minimal load balancing by assigning the majority of the computation to a single GPU while distributing only a small fraction of the workload to the remaining GPUs. As a result, one GPU becomes heavily burdened with the computation, while the other three GPUs remain largely idle for most of the execution process. This imbalance leads to inefficient resource utilization, causing the distribution computation to become nearly sequential. Consequently, PLACETO exhibits the slowest execution time among the tested approaches.

CRITICAL PATH makes a better attempt at load balancing by distributing the computational workload more evenly across multiple GPUs. However, its performance is negatively impacted by inefficient assignment decisions. Specifically, CRITICAL PATH does not take into account the previous data locations when determining where to assign computations. As a result, it frequently places a node’s

computation on a GPU different from the one holding its input data. This misalignment introduces unnecessary data transfers between GPUs, as all input data must first be moved to the newly assigned GPU before computation can begin. The added communication overhead and the delays caused by data transfers contribute to a slowdown in execution time, ultimately reducing the overall efficiency of the system.

Both ENUMERATIVEOPTIMIZER and DOPPLER effectively mitigate the inefficiencies observed in CRITICAL PATH by ensuring that the consumer of an operation is assigned to one of the GPUs where the corresponding input data is already located. This strategy reduces unnecessary data transfers, leading to improved execution performance. However, ENUMERATIVEOPTIMIZER adopts a more conservative strategy by prioritizing data locality over load balancing. Its cost model assigns a high penalty to communication overhead, often favoring keeping computations and their subsequent consumers on the same GPU. While this minimizes data transfer costs, it sometimes results in an uneven workload distribution, with certain GPUs handling more tasks than others.

In contrast, DOPPLER demonstrates the most effective load-balancing strategy among all four approaches. As evidenced in the performance profile, after an initial stage of communication, DOPPLER achieves consistently higher GPU utilization throughout the majority of the execution process. By intelligently distributing workloads while considering both communication cost and GPU availability, DOPPLER maximizes efficiency, ensuring that all GPUs contribute effectively to the computation. This balanced approach allows DOPPLER to outperform other methods in terms of overall execution speed and resource utilization.

## E.4 Llama-Layer Assignment Visualizations

We show the best assignment we found for four methods on the LLAMA-LAYER computation graph: CRITICAL PATH (Figure 16), PLACETO (Figure 15), ENUMERATIVEOPTIMIZER (Figure 13), DOPPLER (Figure 14).

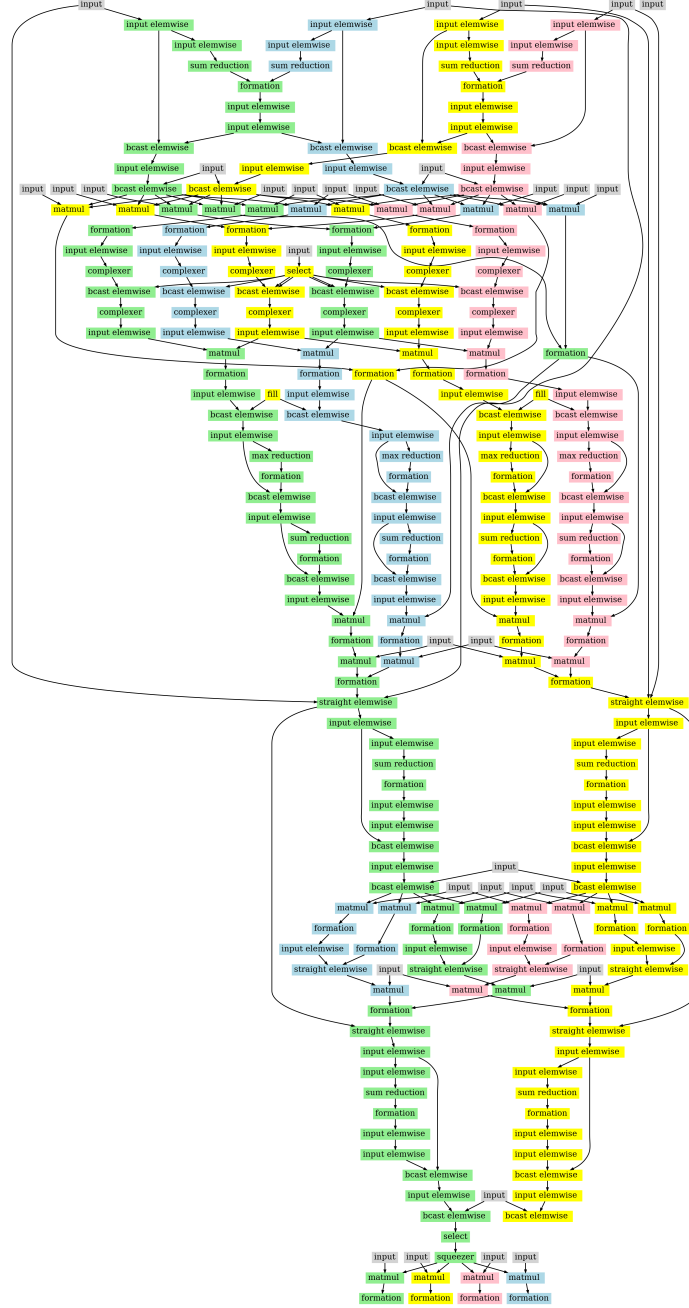


Figure 13: Assignment found by EnumerativeOptimizer for LLAMA-LAYER

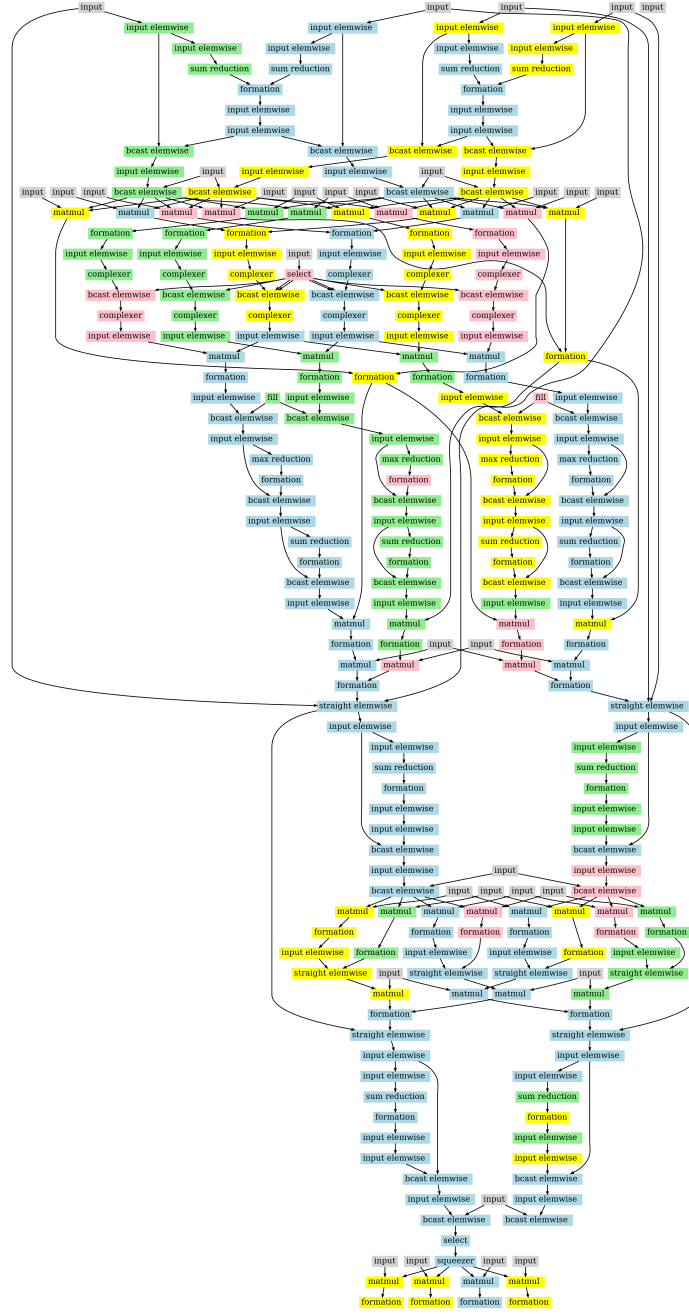


Figure 14: Assignment found by DOPPLER for LLAMA-LAYER

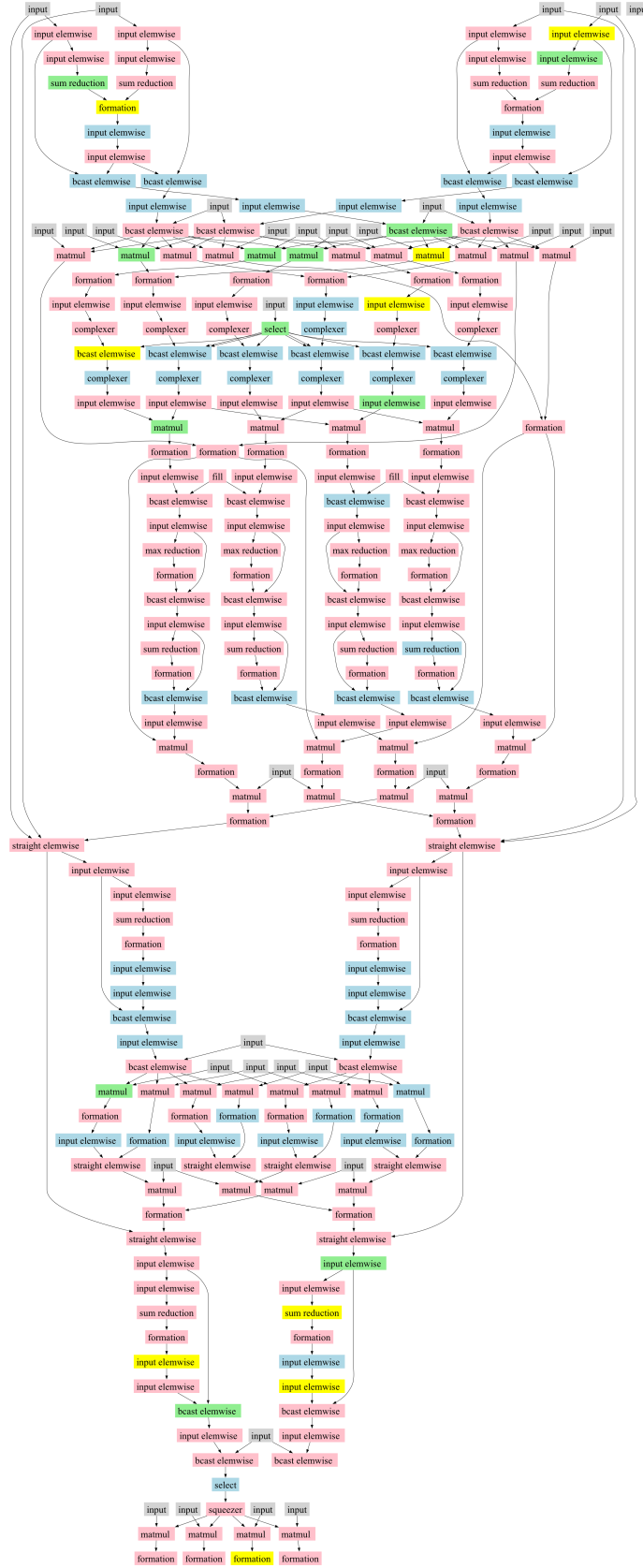


Figure 15: Assignment found by PLACETO for LLAMA-LAYER



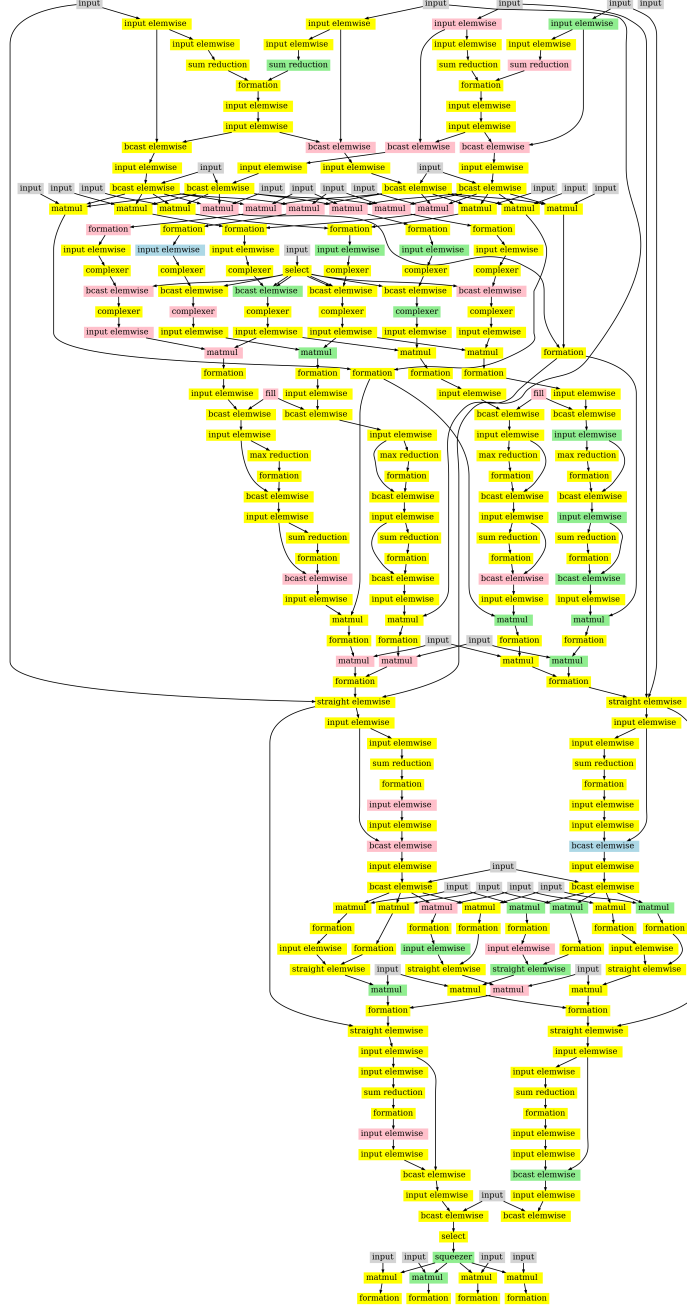


Figure 16: Assignment found by CRITICAL PATH for LLAMA-LAYER

## F Synchronous system Configuration

In Table 1, we run CHAINMM using ScalaPack and FFNN using Pytorch Lightning with tensor parallel on 4 NVIDIA Tesla P100 GPUs with 16GB memory each.

## G Visualizations for Work-conserving system versus bulk-synchronous system

Table 17 shows a comparison of kernel function executions and memory operations in a bulk-synchronous scheduling system versus a work-conserving scheduling system. The green bars denote CUDA kernel operations—for example, matrix multiplications or matrix additions on each GPU, and the red bars indicate memory operations—for example, data transfer between GPU memories. The visualization shows an initial round of kernel operations on all GPUs, followed by data transfers between GPU 0 and GPU 2, and between GPU 1 and GPU 3, before another round of kernel operations.

In a bulk-synchronous system, all data transfer occurs through collective communications, in which all devices synchronize to start and end data transfers simultaneously before proceeding to the final round of kernel executions. In the bulk-synchronous scheduling GPU execution timeline, the two vertical bars in blue represent the start and end times of the collective communications. In contrast, a work-conserving system allows each GPU to start its data transfer immediately after completing its kernel execution. Once each GPU receives the necessary data (eg, GPU 0 receiving data from GPU 2), it immediately proceeds with kernel operations without waiting for unrelated transfers (such as between GPU 1 and GPU 3) to finish. The visualization shows that the work-conserving system completes the same tasks in less time than the bulk-synchronous system.

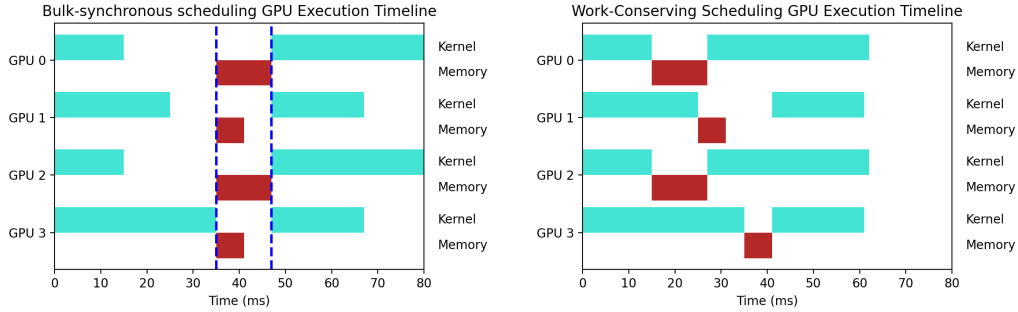


Figure 17: Kernel and memory operations across four GPUs under two scheduling strategies: bulk-synchronous (left) and work-conserving (right). In the bulk-synchronous system, collective communication occurs in a synchronized fashion, where the start and end times are denoted in vertical blue lines (left), whereas the work-conserving system performs communication fully asynchronously without synchronous start and end times for communications (right). As a result, the work-conserving system completes the operations in less time.

## H More Ablation Studies

We conduct additional ablation studies on (1) the simulator implementation, (2) random seeds used in training dual policy, (3) the number of message-passing rounds per episode, and (4) the inclusion of pre-training stages on PLACETO. We aim to evaluate the performance and training efficiency of our three-stage training approach with dual policy design compared with alternatives.

### H.1 Simulator Ablation Studies

We compared the simulated and real system execution times for the same device assignments in the following plots. **We hypothesize that the simulator serves as a cost-effective way to approximate system execution times without sacrificing significant precision.** On the top in Figure 18, we show the running times for both the simulator and the real system for training the dual policy on ChainMM computation graph via imitation learning. We observe that the simulator tends to overestimate the running time compared to the real system running time and has some trouble differentiating between assignments with similar running times. However, the simulator provides approximate running times

that follow the same trend as the real system (eg, high-quality assignments tend to have shorter running times, and low-quality ones exhibit longer running times). On the bottom in Figure 18, we show a statistical analysis comparing the performance of the simulator with the real system under the same setup. We find a Pearson coefficient of 0.79 and a Spearman coefficient of 0.69. This ablation study demonstrates that the simulator offers a cost-effective way to approximate system execution times.

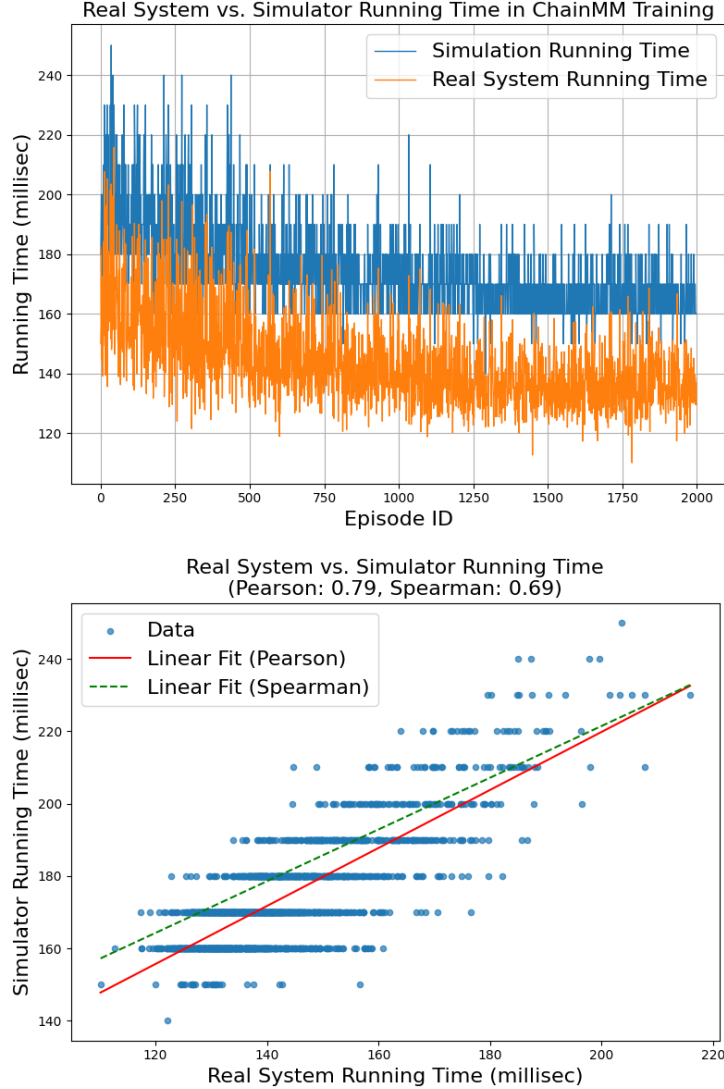


Figure 18: (left) A line chart showing a comparison between the simulator running time and the real system running time throughout training. (right) A scatter plot showing the simulator running time versus the real system running time with Pearson and Spearman fitting lines.

## H.2 Experiment with Random Seeds

In this study, we aim to test **the hypothesis that the best assignment found by our approach DOPPLER remains consistent across different random seeds during training**. Due to the cost of training, we are unable to run experiments multiple times with random seeds for all computational graphs and methods. Therefore, we conduct five training runs of DOPPLER-SYS with different seeds on ChainMM computation graph to test this hypothesis. This experimental setup—including computation graph, dual policy architectures, and training hyperparameters—is identical across runs, differing only in the random seeds. For each training run, we evaluate the best-found assignment over

10 system executions and report the mean and standard deviation in Table 5. The results show that DOPPLER achieves consistent performance across different random seeds.

Model	Run1	Run2	Run3	Run4	Run5
ChainMM	$123.2 \pm 3.7$	$119.6 \pm 2.2$	$122.7 \pm 2.1$	$123.9 \pm 2.5$	$121.7 \pm 0.9$

Table 5: Experiment running DOPPLER using different random seeds on CHAINMM computation graph. We test the best assignment found at the end of the training across different seeds with 10 system runs and report the mean and standard deviation of the system running time (in milliseconds) for each assignment.

### H.3 Message-Passing Ablation Studies

To enhance training efficiency for large computation graphs, we apply a message-passing round on the graph once per MDP episode instead of once per MDP step. For applying message-passing once per MDP step, this means that the number of message-passing rounds per episode equals the number of nodes in the graph. **We hypothesize that this modification has a negligible impact on DOPPLER’s convergence but significantly reduces training time—proportional to the number of nodes in the computation graph.** We conduct this ablation study on the ChainMM computation graph using the simulator to save time, since per-step message-passing incurs prohibitively high training costs.

	DOPPLER-SIM	DOPPLER-SIM-mpnn-per-step
Best assignment	$122.5 \pm 4.0$	$121.7 \pm 3.2$
Number of episodes	3425	963
Number of message passing	3425	107,856
Run time reduction	0.7%	
Extra message-passing	3049.1%	

Table 6: Running time (in milliseconds) for the best device assignment found at the end, along with the number of message-passing steps conducted until finding the best assignment. The reported time for the best assignment includes both the average and standard deviation of the system running time over 10 system rounds. DOPPLER-SIM refers to performing message passing on the computation graph per MDP episode, while DOPPLER-SIM-mpnn-per-step denotes conducting message-passing per MDP step within each episode.

In each MDP step within an episode, we assign a device to the currently selected node. Therefore, for the DOPPLER-SIM-mpnn-per-step approach, the number of message-passing rounds per episode equals the number of nodes in the computation graph. The ChainMM computation graph consists of 112 nodes. Table 6 shows that the best assignments—reported in the first row by their running times—were found at episode 3425 for DOPPLER-SIM and at episode 963 for DOPPLER-SIM-mpnn-per-step. Although the best assignment was found in fewer episodes with DOPPLER-SIM-mpnn-per-step, completing 963 episodes took significantly more wall-clock time than 3425 episodes for DOPPLER-SIM, because message-passing took the majority of time during training.

We evaluate the efficiency of the two approaches based on the number of message-passing rounds required to find the best assignment. DOPPLER-SIM performs 3425 message-passing operations (one per episode), while DOPPLER-SIM-mpnn-per-step conducts  $963 \text{ episodes} \times 112 \text{ nodes} = 107,856$  message-passing operations (one per MDP step, or equivalently, per node in the computation graph). DOPPLER-SIM-mpnn-per-step achieves a 0.7% reduction in runtime for the best assignment compared to DOPPLER-SIM, but at the cost of 3049.1% more message-passing. Therefore, these results support our hypothesis that the modified approach has greatly reduced the training time with negligible impact on the performance.

#### H.4 PLACETO Ablation Studies

We conduct an ablation study on policy design for learning device assignments in both DOPPLER and PLACETO, explicitly including pre-training stages for PLACETO to isolate the effect of the underlying policy design from the benefits of pre-training. **We hypothesize that the dual policy design in DOPPLER outperforms PLACETO regardless of the inclusion of the training stages.** To test our hypothesis, we pre-train PLACETO policy using imitation learning and compare it with DOPPLER-SIM, which is trained using the imitation learning stage (Stage I) and the simulation-based RL stage (Stage II).

	PLACETO-pretrain	PLACETO	DOPPLER-SIM	DOPPLER-SYS
Best Assignment	$99.0 \pm 5.7$	$126.3 \pm 5.8$	$49.9 \pm 1.1$	$47.4 \pm 0.7$

Table 7: The mean and standard deviation of the running time (in milliseconds) for the best assignment found for DOPPLER, compared to PLACETO and its pre-training version, PLACETO-pretrain, over 10 system runs. The results indicate that even with the pre-training stage, PLACETO-pretrain performs worse than DOPPLER-SIM.

Table 7 shows that DOPPLER discovers more effective device assignments than PLACETO. This result isolates the impact of the training stages and support the claim that DOPPLER’s dual policy design outperforms the policy design in PLACETO.

### I DOPPLER’s Experiments on Different Hardware Configurations

The experiments so far demonstrate that DOPPLER outperforms the alternatives on four Tesla P100 GPUs, each with 16GB of memory. We hypothesize that DOPPLER could find better device assignments than alternatives across different hardware configurations. In this Section, we conduct experiments with DOPPLER and other methods under 1) varying GPU memory size on four P100 GPUs, and 2) different numbers and types of GPUs. Each experimental setup is described in the following two subsections.

#### I.1 Experiments with restricted GPU memory

**We aim to test the hypothesis that DOPPLER can adapt to the hardware setups with restricted GPU memory.** Table 8 shows results on four NVIDIA P100 GPUs, each restricted to use 8 GB out of their 16 GB total memory. DOPPLER learns to adapt to memory constraints, achieving up to 49.6% and 18.6% runtime reductions compared to the best baseline and ENUMERATIVEOPTIMIZER, respectively, while heuristics fail to adapt due to dynamic memory allocations in WC systems. These results confirm that DOPPLER can adapt to restricted memory settings.

MODEL	1 GPU	4 GPUs				RUNTIME REDUCTION	
		CRITICAL PATH	PLACETO	ENUMOPT.	DOPPLER-SYS	BASELINE	ENUMOPT.
CHAINMM	$439.8 \pm 4.6$	$310 \pm 4.9$	$243.5 \pm 5.9$	$133.5 \pm 10.4$	<b><math>122.6 \pm 2.2</math></b>	49.6%	8.2%
FFNN	$148.2 \pm 19.4$	$225.8 \pm 19.4$	$126.8 \pm 5.7$	$49.2 \pm 0.9$	<b><math>46.0 \pm 0.8</math></b>	63.7%	6.5%
LLAMA-BLOCK	$465.1 \pm 7.8$	$216.8 \pm 4.6$	$433.5 \pm 6.2$	$233.8 \pm 8.1$	<b><math>190.2 \pm 11.2</math></b>	12.3%	18.6%
LLAMA-LAYER	$482.6 \pm 9.4$	$292.5 \pm 5.1$	$302.1 \pm 20.2$	$172.8 \pm 4.3$	<b><math>154.0 \pm 3.7</math></b>	47.4%	10.9%

Table 8: Real engine execution times (in milliseconds) for assignments identified by our approaches (EnumerativeOptimizer, Doppler-SYS) using 4 GPUs with access to 8G out of 16G GPU memory for each GPU compared against those produced using 1 GPU and by two baselines (CRITICAL PATH and PLACETO). The results show that Doppler-SYS outperforms all baselines across all settings.

#### I.2 Experiments on different numbers and types of GPUs

**We aim to test the hypothesis that DOPPLER can find better device assignments regardless of the number and type of GPUs in the server.** Table 9 presents results running various computation graph architectures on eight NVIDIA V100 GPUs, each with 32 GB of memory. The setup consists of

two device meshes, each fully interconnected via NVLinks, with a total of four additional NVLinks spanning between the meshes. We observed that DOPPLER effectively leverages NVLink to minimize inter-mesh data transfer. We show that DOPPLER achieves up to 67.7% runtime reduction compared to the existing baseline, and up to 19.3% compared to ENUMERATIVEOPTIMIZER.

MODEL	1 GPU	8 GPUs			RUNTIME REDUCTION	
		CRITICAL PATH	ENUMOPT.	DOPPLER-SYS	BASELINE	ENUMOPT.
CHAINMM	83.5 $\pm$ 4.1	69.6 $\pm$ 2.6	33.5 $\pm$ 2.5	<b>32.1</b> $\pm$ 0.7	53.9%	4.1%
FFNN	51.4 $\pm$ 1.8	50.0 $\pm$ 6.0	20.0 $\pm$ 2.6	<b>16.2</b> $\pm$ 2.3	67.7%	19.3%
LLAMA-BLOCK	154.4 $\pm$ 6.3	117.6 $\pm$ 6.0	<b>109.6</b> $\pm$ 4.2	109.7 $\pm$ 3.0	6.7%	-0.1%
LLAMA-LAYER	105.0 $\pm$ 4.8	105.4 $\pm$ 4.2	97.5 $\pm$ 1.1	<b>90.6</b> $\pm$ 4.1	13.7%	7.1%

Table 9: Real engine execution times (in milliseconds) for assignments identified by our approaches (EnumerativeOptimizer, Doppler-SYS) using 8 V100 GPUs compared against those produced using 1 GPU and by one baseline (CRITICAL PATH). The results show that Doppler-SYS outperforms the alternatives in 3 out of 4 settings.

## J Details on the three training stages

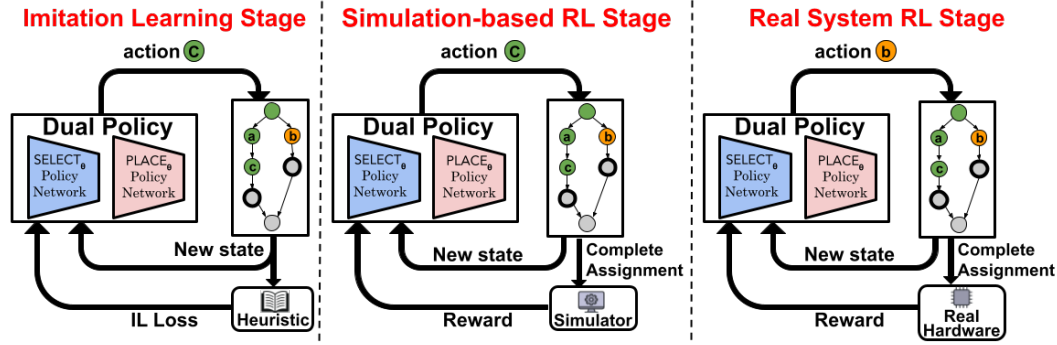


Figure 19: Three-stage framework for training DOOPPLER cost-effectively by combining imitation learning, simulation-based RL, and real-system RL.

Figure 19 illustrates the workflow of the three training stages: imitation learning stage, simulation-based RL stage, and real system RL stage. Dual policy is trained sequentially through these three stages.

During the imitation learning stage, the computation graph produces a new state at each step, which describes the current assignment in the graph. This state is provided to both the dual policy and the heuristic method. Dual policy then produces an action consisting of a node and its corresponding device. The computation graph applies the action taken by the dual policy and transitions to a new state. At each MDP step, a loss is computed based on the action taken by the heuristic. The cumulative loss over the entire episode is then used to update the dual policy at the end of each episode.

During the simulation-based RL stage, the heuristic is replaced by a simulator that provides a reward based on the computation graph with a complete device assignment. The simulator is invoked only at the terminal step, once all nodes in the computation graph have been assigned devices. At this point, the simulator executes the computation graph with the full assignment, following Algorithm 1, and returns a reward to update the dual policy.

In the real system RL stage, the simulator is replaced by the real hardware which executes the computation graph directly—without simulated data—following Algorithm 1. In this stage, the real hardware actively serves real-world user requests. The reward is derived from the observed execution time of the assignment produced by the dual policy.

## **K Discussion on scaling to much larger dataflow graphs**

While there is no reason that the method cannot scale, in practice, very large graphs tend to be constructed of repeating graph structures (transformer blocks, for example). In practice, one could use DOPPLER to learn to place a transformer block and then simply repeat that placement in each repeated structure during deployment, using the overall running time to compute a reward. Our method also incorporates an efficient training mechanism that reduces the number of message-passing rounds—by a factor proportional to the number of graph nodes—thereby significantly decreasing training time, as described in Appendix H.3.